J. Am. Chem. Soc. **1990**, *112*, 8776-8789

Structure of Lithium Isodicyclopentadienide and Lithium Cyclopentadienide in Tetrahydrofuran Solution. A Combined NMR, IGLO, and MNDO Study

Leo A. Paquette,*,† Walter Bauer,‡ Mark R. Sivik,† Michael Bühl,‡ Martin Feigel,‡ and Paul von Ragué Schleyer‡

Contribution from Evans Chemical Laboratories, The Ohio State University, Columbus, Ohio 43210, and Institut für Organische Chemie der Universität Erlangen-Nürnberg, Henkestrasse 42, D-8520 Erlangen, Federal Republic of Germany. *Received February 14, 1990*

Abstract: One- and two-dimensional NMR shows lithium isodicyclopentadienide **1** to exist as a monomer–dimer equilibrium in tetrahydrofuran (THF) at low temperatures. In the monomer, a contact ion pair, lithium is located at the exo face (**4**). The dimer consists of lithium "sandwiched" between the exo faces of two anion moieties (**6**). The sandwiched lithium in **6** is highly shielded and resonates at −12.8 ppm. The experimental lithium chemical shifts are reinforced by IGLO calculations. Line-shape analysis of the temperature-dependent ^{6}Li NMR spectra reveals two kinetic processes: rapid exchange of $[Li(THF)_4]^+$ with monomer-bound lithium and slower exchange between sandwiched and monomer-bound lithium. MNDO calculations confirm the NMR results of the relative stabilities of the exo lithio isomers of monomeric and dimeric **1** over their endo lithio counterparts. In addition, MNDO predicts contact ion pairs to be favored for both the monomeric and the dimeric species. At room temperature the monomer **4**–dimer **6** equilibrium is apparently shifted toward the monomer side. This might explain earlier experimental findings of mainly exo electrophilic attack on **1** at +25 °C over preferred endo attack at −78 °C. Lithium cyclopentadienide **5** is found to behave similarly to **1** in THF solution, i.e., a monomer–"sandwich" dimer equilibrium is indicated due to the exceptional upfield ^{6}Li chemical shifts. However, the exchange processes are considerably faster than those found for **1**.

Introduction

As early as 1983 we noticed that the stereoselective reaction of lithium isodicyclopentadienide (Li–isodiCp, **1**) with methyl iodide[1a] and with trimethylchlorosilane[1b] shows an amazing dependence on the temperature. Electrophilic attack at the endo face occurs at −78 °C in tetrahydrofuran (THF) solution whereas **1** is attacked from the exo face at room temperature (Scheme Ia,b). A similar stereoselectivity is exhibited by the reaction of **1** with $CpTiCl_3$[2] (Scheme Ic).

Several experiments confirmed kinetic control of these reactions: the products **2** and **3** formed are thermodynamically stable;[1,2] e.g., when **2c** is mixed in equimolar amount with **3c**-d_3 (deuteration in the Cp ring) and refluxed for 18 h in THF, no deuterium crossover is detected.[2] In order to rationalize these findings we have now investigated the structure of the reactive intermediate, Li–isodiCp **1**, under conditions similar to those of the quench experiments, i.e., in THF at low temperatures and at room temperature, and at comparable concentrations. Both calculational (MNDO, IGLO) and experimental methods (NMR, cryoscopy) provided many new insights into the nature of this species.

Lithium Isodicyclopentadienide 1

NMR Spectral Assignments. All our NMR studies employed 96% ^{6}Li-enriched lithium and THF-d_8. For convenience we use the numbering and stereochemical assignments for Li-isodiCp shown in Figure 1.

When **1** is dissolved in THF-d_8, the ^{1}H, ^{13}C, and ^{6}Li NMR spectra at +25 °C show a single set of signals. This is compatible with either the presence of one species or a rapid exchange (on the NMR time scale) between different aggregates and/or isomers. The assignment of the ^{1}H NMR spectrum (Figure 2a) is straightforward. As usual in norbornane derivatives, the signal of H8,9(endo) appears upfield from H8,9(exo).[3] H10(syn) and H10(anti) can be assigned by NOE difference spectroscopy:[4] when the signal of H8,9(exo) is irradiated, a positive NOE is observed for the signal at 1.42 ppm, which therefore must be due to H10(anti) (Figure 2b).

Scheme I

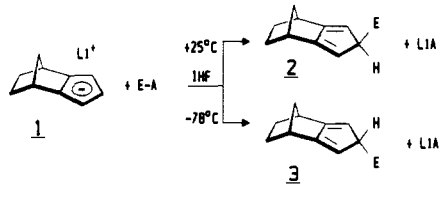

a) E = CH_3, A = I

b) E = $(CH_3)_3Si$, A = Cl

c) E = $CpTiCl_2$, A = Cl

Table I. ^{1}H NMR Chemical Shifts (δ, ppm) of Li–isodiCp **1** in THF-d_8 at +25 and −100 °C (0.86 M)

		−100 °C	
H	+25 °C	monomer **4**[a]	dimer **6**[b]
1,7	3.03	3.04	2.89
3,5	5.19	5.20	4.87
4	5.31	5.33	4.94
8,9 exo	1.60	1.61	1.51
8,9 endo	0.83	0.79	0.66
10 syn	1.50	1.51	1.81
10 anti	1.42	1.39	1.31

[a] Major species. [b] Minor species.

Table II. ^{13}C NMR Chemical Shifts (δ, ppm) of Li–isodiCp **1** in THF-d_8 at +25 and −100 °C (0.86 M)

		−100 °C	
C	+25 °C	monomer **4**[a]	dimer **6**[b]
1,7	41.67	41.99	41.43
2,6	129.07	127.83	127.36
3,5	93.83	92.51	93.63
4	102.25	103.09	102.39
8,9	30.91	31.27	31.11
10	51.87	51.10	51.57

[a] Major species. [b] Minor species.

The assignment of the ^{13}C NMR spectrum of **1** at +25 °C in THF-d_8 follows easily from ^{1}H,^{13}C shift correlation spectroscopy

† Ohio State University.
‡ Universität Erlangen-Nürnberg.

0002-7863/90/1512-8776$02.50/0

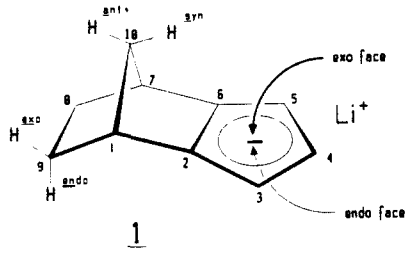

Figure 1. Numbering and stereochemical assignments in lithium isodicyclopentadienide **1** used in this paper. Underlined letters indicate abbreviations used.

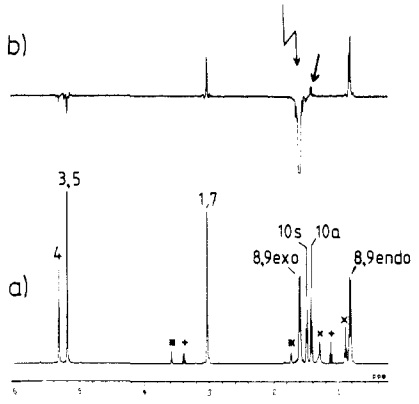

Figure 2. ^{6}Li-isodiCp **1** in THF-d_8. Conditions: 0.68 M, +25 °C; *, solvent signal (THF-d_8); x, hexane; +, diethyl ether. (a) Normal ^{1}H NMR spectrum. (b) Difference NOE spectrum, irradiation of H8,9-(exo); the arrow indicates a positive NOE at H10(anti).

(not shown).[5,6] The ^{1}H and ^{13}C NMR chemical shifts of **1** at +25 °C are given in Tables I and II. The ^{6}Li NMR spectrum of **1** at +25 °C consists of one sharp signal at −8.30 ppm. This unusual upfield chemical shift will be discussed below.

Upon cooling, dynamic phenomena are observed in the NMR spectra. At −100 °C, two sets of signals approximately in a 2:1 ratio for a 0.8 M THF-d_8 solution are observed in the ^{1}H and ^{13}C NMR spectra. These must be due either to different stereoisomers, e.g., monomers with lithium located at the exo and at the endo face, or to different aggregates, e.g., a monomer–dimer equilibrium. The following findings show the latter to be likely.

The ^{1}H and ^{13}C NMR spectral assignments were achieved by using two-dimensional techniques. Figure 3 shows the COSY contour plot[6,7] of **1** in THF at −100 °C. Therein the connectivities of protons within the different aggregates can be determined easily. Note the relatively strong downfield shift of H10(syn) of the minor species. This will be discussed subsequently.

In the ^{1}H,^{13}C shift correlated spectrum (Figure 4), the less trivial assignments of the diastereotopic protons H8,9(endo) and H10(syn,anti) are confirmed by their cross peaks with the corresponding carbon signals. The assignment of H10(syn) and H10(anti) was confirmed by a 2D NOESY spectrum[6] (not shown). Therein, NOE cross peaks can be detected between the resonances of H10(anti) and H8,9(exo) for both species. The ^{1}H

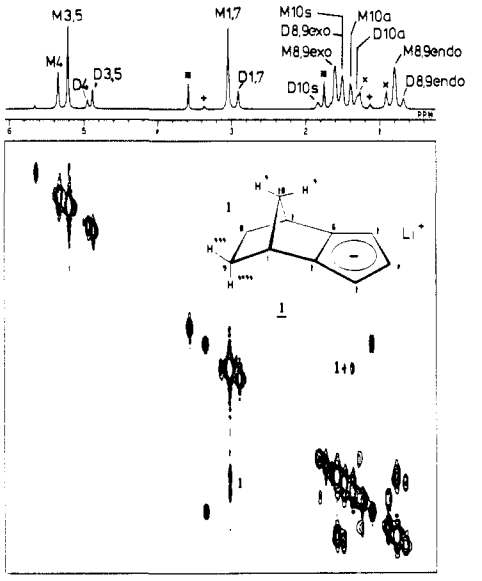

Figure 3. COSY contour plot of **1** in THF-d_8 at −100 °C, 0.35 M. For numbering, see Figure 1. M, monomer **4**; D, dimer **6**; *, solvent signal (THF-d_8); x, hexane; +, diethyl ether.

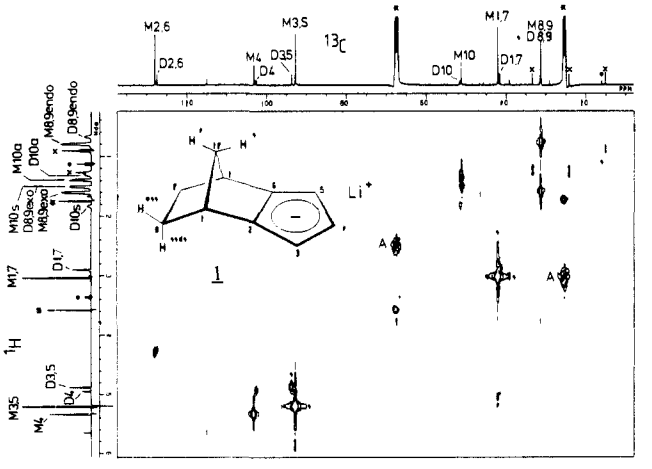

Figure 4. ^{1}H,^{13}C shift correlation spectrum of **1**, contour plot, in THF-d_8 at −100 °C, 0.35 M. For numbering, see Figure 1. M, monomer **4**; D, dimer **6**; A, artificial cross peak; *, solvent signal (THF-d_8); x, hexane; +, diethyl ether; the one-dimensional proton spectrum is displayed with slight resolution enhancement (Gaussian window).

and ^{13}C NMR chemical shifts of the two species observed at −100 °C are summarized in Tables I and II.

The ^{6}Li NMR spectrum of **1** in THF at −100 °C (0.8 M solution) shows *three* signals (δ = −1.10, −7.64, and −12.78 ppm; cf. Figure 5). As the ^{1}H and ^{13}C NMR spectra indicate the presence of only two compounds, two of these signals must be due to the same species. This is corroborated by equal intensities of the "outer" signals at −1.10 and −12.78 ppm as well as by identical changes in the intensities of these signals when the concentration is varied (Figure 5). Chemically nonequivalent lithium sites within the same molecule have been reported, e.g., by us (for the reaction product of *n*-BuLi with tolane,[8] as well as by Fraenkel[9] and by Günther.[10]

The range of Li chemical shifts is restricted to ca. −2 to +2 ppm for most organolithium compounds studied so far. Exceptions are found when the lithium cation is located in regions of high magnetic anisotropy of the anion moiety. Thus, apparently due

(1) (a) Paquette, L. A.; Charumilind, P.; Kravetz, T. M.; Böhm, M. C.; Gleiter, R. *J. Am. Chem. Soc.* **1983**, *105*, 3126. (b) Paquette, L. A.; Charumilind, P.; Gallucci, J. C. *J. Am. Chem. Soc.* **1983**, *105*, 7364.

(2) (a) Paquette, L. A.; Moriarty, K. J.; Meunier, P.; Gautheron, B.; Crocq, V. *Organometallics*, **1988**, *7*, 1873. (b) Paquette, L. A.; Moriarty, K. J.; Meunier, P.; Gautheron, B.; Sornay, C.; Rogers, R. D.; Rheingold, A. L. *Organometallics* **1989**, *8*, 2159.

(3) Moritz, A. G.; Sheppard, N. *Mol. Phys.* **1962**, *5*, 361.

(4) Neuhaus, D.; Williamson, M. P. *The Nuclear Overhauser Effect in Structural and Conformational Analysis*; VCH Publishers: New York, 1989.

(5) Bodenhausen, G.; Freeman, R. *J. Magn. Reson.* **1977**, *28*, 471. Freeman, R.; Morris, G. A. *Chem. Commun.* **1978**, 684. Bodenhausen, G.; Freeman, R. *J. Am. Chem. Soc.* **1978**, *100*, 320.

(6) Kessler, H.; Gehrke, M.; Griesinger, C. *Angew. Chem.* **1988**, *100*, 507; *Agnew. Chem., Int. Ed. Engl.* **1988**, *27*, 490.

(7) Aue, W. P.; Bartholdi, E.; Ernst, R. R. *J. Chem. Phys.* **1976**, *64*, 2229.

(8) Bauer, W.; Feigel, M.; Müller, G.; Schleyer, P. v. R. *J. Am. Chem. Soc.* **1988**, *110*, 6033.

(9) Fraenkel, G.; Hallden-Abberton, M. P. *J. Am. Chem. Soc.* **1981**, *103*, 5657.

(10) Günther, H.; Moskau, D.; Dujardin, R.; Maercker, A. *Tetrahedron Lett.* **1986**, *27*, 2251.

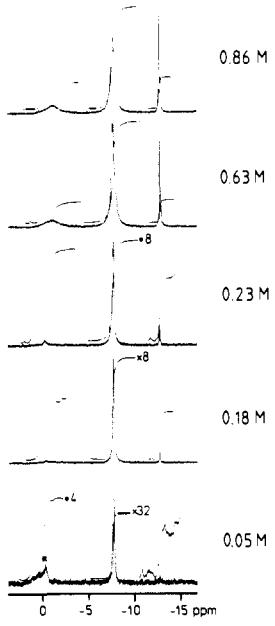

Figure 5. ^{6}Li NMR spectra of Li-isodiCp **1** at different concentrations in THF-d_8 at −100 °C. *, impurity signal; the integral heights have to be multiplied by the indicated values.

to ring current phenomena, the ^{7}Li resonance was found to be strongly shifted upfield in cyclopentadienyllithium (δ = −8.37 ppm in THF) and in indenyllithium (δ = −8.99 ppm in Et_2O).[11] Moreover, Exner et al.[12] found extremely high ^{7}Li upfield shifts in (9-(2-hexyl)fluorenyl)lithium (δ = −13.3 ppm in benzene). This "double" shielding was attributed to lithium "sandwiching" between two aromatic rings.

Recently, Jutzi et al.[13] reported ^{7}Li NMR chemical shifts of substituted cyclopentadienyllithium derivatives in benzene solution with various added bases. These range between −8.2 and −12.5 ppm, indicating analogous ring current effects.

Similar exceptional high field shifts for nuclei sandwiched between two cyclopentadienyl rings also are observed for silicon. Thus, Jutzi et al. found an extreme upfield shift for ^{29}Si (δ = −398 ppm) in decamethylsilicocene.[14]

Our ^{6}Li chemical shifts for **1** (δ = −7.64 and −12.78 ppm) at low temperatures are close to the values reported in refs 11 and 12. Hence, in THF-d_8 solution at −100 °C, **1** consists of a monomer–dimer equilibrium mixture. In the monomer, ^{6}Li is located above the cyclopentadienyl ring and resonates as a single peak at −7.64 ppm. Structures **4** and **5** with Li at the exo or the endo face would account for this behavior. We will show in the following that the *exo* monomer **4** is actually involved.

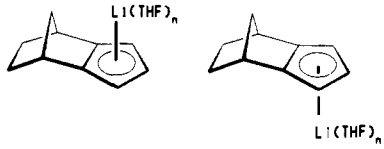

4 **5**

The dimer is believed to consist of a lithium "ate" complex (triple ion) with a "sandwiched" lithium cation, resonating at −12.78 ppm. The counterion to the sandwiched anion is indicated to be a "naked" lithium cation, which is (presumably) tetrahedrally surrounded by four THF ligands. Alternatively, this lithium site might refer to lithium that is "externally" bound to the dimer anion sandwich. This type of contact ion pair (CIP) will be discussed below. The ^{6}Li chemical shift of this cation, −1.10 ppm, is in the "normal" range. Thus, e.g., structure **6** or **7** is suggested for this

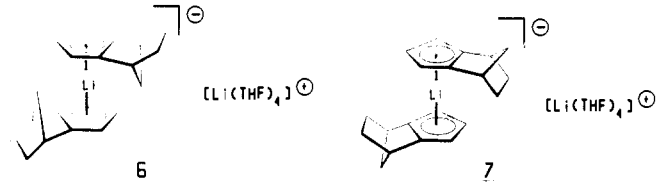

6 **7**

dimer. These differ in the location of lithium on the π faces: **6** is a bis exo and **7** is a bis endo sandwich. It will be shown below that we presumably observe the bis exo dimer **6** in THF-d_8 at −100 °C.

In the solid state only one example of lithium sandwiched between two aromatic rings has been reported. Rewicki and Dietrich[15] found lithium indenofluorene to adopt the dimer structure **8**. However, Fraenkel has presented NMR evidence

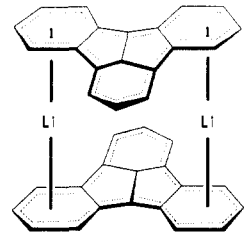

8

for π sandwich structures in solution.[9]

The monomer–dimer equilibrium found for **1** in THF-d_8 at low temperatures is highly concentration dependent; with decreasing overall concentration of **1**, the amount of the monomer increases strongly. This is consistent, e.g., with equilibrium 1.

$$\text{dimer } \mathbf{6} + (2n-4)\text{THF} \rightleftharpoons 2\text{monomer } \mathbf{4} \qquad (1)$$

Figure 5 shows a series of concentration-dependent ^{6}Li NMR spectra of **1** in THF-d_8 at −100 °C. These are quite similar to Fraenkel's findings for **9**.[9] This species was shown to consist of

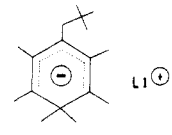

9

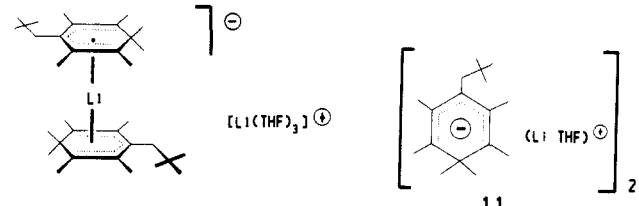

10 **11**

two distinct aggregates in THF, one of which was claimed to be a sandwich **10** analogous to our proposed dimers **6** and **7**. The second species was believed to be a "partially solvated tight ion pair dimer" **11**. Due to chemical nonequivalence of the two lithium sites in **10**, a total of three peaks was observed in the ^{7}Li NMR of **10** and **11**. With increasing concentrations of THF the **10**–**11** equilibrium was shifted away from the dimer **10**.

An analogous formation of triple ions was recently reported by Collum[16] for lithiated hydrazones. Therein, only 50% of lithium

(11) Cox, R. H.; Terry, H. W., Jr. *J. Magn. Reson.* **1974**, *14*, 317. Cox, R. H.; Terry, H. W., Jr.; Harrison, L. W. *J. Am. Chem. Soc.* **1971**, *93*, 3297. Note that the sign of Li chemical shifts therein is opposite to the now agreed convention of δ < 0 for high-field (low-frequency) shifts.

(12) Exner, M. M.; Waack, R.; Steiner, E. C. *J. Am. Chem. Soc.* **1973**, *95*, 7009.

(13) Jutzi, P.; Leffers, W.; Pohl, S.; Saak, W. *Chem. Ber.* **1989**, *122*, 1449.

(14) Jutzi, P.; Holtmann, U.; Kanne, D.; Krüger, C.; Blom, R.; Gleiter, R.; Hyala-Kryspin, I. *Chem. Ber.* **1989**, *122*, 1629. In an earlier paper (Jutzi, P.; Kanne, D.; Krüger, C. *Angew. Chem.* **1986**, *98*, 163; *Angew. Chem., Int. Ed. Engl.* **1986**, *25*, 164), this resonance was erroneously reported to appear at δ = −577 ppm (Jutzi, P., personal communication, 1989).

(15) Bladauski, D.; Broser, W.; Hecht, H.-J.; Rewicki, D.; Dietrich, H. *Chem. Ber.* **1979**, *112*, 1380.

was found to be complexed by cryptand C[2.1.1], leading to a system $[R_2Li]^-\{Li^+C[2.1.1]\}$, where R is a hydrazone anion. Likewise, Jackman detected a triple ion of type $[R_2Li^-[Li(HMPA)_4]^+$, R = PhN(*i*-Pr)$^-$ in diethyl ether solution, which is in equilibrium with a monomer RLi.[17]

The number of THF ligands associated with the monomer (the value of *n* in eq 1) should be extractable by plotting log ([monomer]^2/[dimer]) vs log [THF].[18] However, as will be shown below (MNDO section), there is an undetermined number of THF molecules associated with the dimer. Hence, our data can only be treated qualitatively.

The temperature dependence of eq 1 plays a key role in the interpretation of the switch in stereoselectivity of electrophilic attack on **1**. In principle, this should be extractable from integration of the NMR spectra. The observed ratio of monomer **4** to dimer **6** remains constant between −108 and −80 °C (within the errors of the integration). Unfortunately, coalescence above ca. −80 °C precludes separate integration of each species at higher temperatures. However, several observations indicate that the equilibrium that forms reaction 1 at +25 °C lies completely on the side of the monomer **4**:

(i) The ^{1}H NMR chemical shifts of **1** in THF at +25 °C are identical with those found for the *monomer* at −100 °C and differ significantly from those of the dimer (see Table I).

(ii) When the concentration of **1** in THF is varied between 0.86 and 0.05 M, the ^{13}C NMR chemical shifts at +25 °C remain *exactly* constant. The ^{1}H NMR chemical shifts of **1** vary only slightly at different concentrations. This is a general phenomenon in ^{1}H NMR spectroscopy[19] and is largely incompatible with an equilibrium between different aggregates.

Thus, it is likely that we are observing only the monomer **4** at +25 °C. This implies that reaction 1 is endothermic (positive ΔH).[20] Similarly, in the equilibrium **10** ⇌ **11** described by Fraenkel[9], the concentration of the "sandwich" dimer **10** decreases with increasing temperatures.

Yet, the available data may still be insufficient to definitely prove the exclusive existence of monomer **4** at +25 °C.

IGLO Results

In order to rationalize the unusual high-field lithium chemical shifts observed for the monomer **4** and the dimer **6**, we calculated the Li shifts in the model structures **12** and **13** using the IGLO

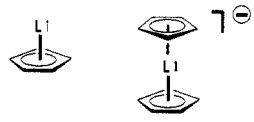

12 C_{5v} **13** D_{5d}

(*i*ndividual *g*auge for *l*ocalized *o*rbitals) method.[22] Provided accurate geometries are employed (experimental structures or those optimized ab initio at an adequate level of theory), this new method has been shown to yield very accurate results, e.g., for ^{13}C NMR chemical shifts.[23]

Table III. IGLO Calculated Absolute Lithium Shielding Constants (σ, ppm) and Chemical Shifts (δ, ppm; Relative to Li^+ ≡ 0.0 ppm) of Lithioorganic Compounds with "Aromatic" Moieties

compd	σ_{Li}	δ_{Li}	compd	σ_{Li}	δ_{Li}
Li^+	95.4	0.0	**14**	98.2	−2.8
Li^-	107.2	−11.8	**15**	97.4	−2.0
12	102.3	−6.9	**16**	98.1	−2.7
13	106.2	−10.8	**17**	98.3	−2.9

By use of a double ζ (DZ) basis set the absolute shielding constants σ for Li in **12** and **13** were found to be 102.3 and 106.2 ppm, respectively. Relative to free Li^+ (σ = 95.4 ppm) this would correspond to chemical shifts of δ = −6.9 ppm for **12** and δ = −10.8 ppm for **13**.[24] Thus, IGLO calculations strongly confirm our assignments of structures **4** and **6** to explain the experimental observations. Interestingly, the shielding constant of lithium in **13** at this level is very close to the calculated value of a "naked" lithium *anion* Li^- (σ = 107.2 ppm, δ = −11.8 ppm)! Higher level IGLO calculations for **12** and **13** confirm these results (for a discussion of Li NMR chemical shifts see ref 23f).

The ab initio optimized geometries of **12** and **13** will be discussed separately below.

For comparison, the chemical shifts for four other compounds, **14**–**17** were calculated by IGLO. We wondered if ring current effects might influence the lithium shielding constants. As the data summarized in Table III show, magnetic anisotropies do not seem to play a significant role in **14**–**17**.

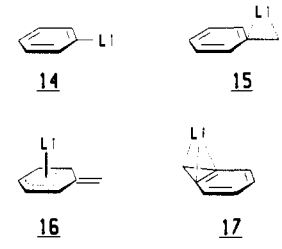

14 **15** **16** **17**

Molecular Weight Determinations

The monomer–dimer equilibrium of **1** was confirmed by a cryoscopic molecular weight determination in THF (mp −108 °C).[25] The measured degree of aggregation, *n* = 1.08 ± 0.04 in a 0.067 *m* solution of **1** in THF, corresponds to a 92% monomer–8% dimer equilibrium. The NMR results are in good agreement: by interpolation of the integrated signals of Figure 5, a 97% monomer–3% dimer equilibrium would be present at this concentration.

Exo–Endo Differentiation

A crucial role in the interpretation of the different quench products of **1** depending on temperature is played by the assignment of the site of the lithium cation. Thus, we need to establish which of the alternatives, **4**/**5** and **6**/**7**, are present in

(16) Galiano-Roth, A. S.; Collum, D. B. *J. Am. Chem. Soc.* **1988**, *110*, 3546.

(17) Jackman, L. M.; Scarmoutzos, L. M.; Porter, W. *J. Am. Chem. Soc.* **1987**, *109*, 6524.

(18) Takaki, U.; Collins, G. L.; Smid, J. *J. Organomet. Chem.* **1978**, *145*, 139.

(19) For a comprehensive overview, see: Suhr, H. *Anwendungen der kernmagnetischen Resonanz in der organischen Chemie*; Springer: Berlin, 1965; p 314 f.

(20) It is often found that in donor solvents equilibria between different aggregates of organolithium compounds are shifted toward the more *aggregated* species upon increasing temperatures, e.g., dimeric/tetrameric *n*-butyllithium.[21] This is commonly attributed to "entropic factors" as the equilibrium side of the higher aggregate contains more particles. This explanation is not correct. Thermodynamics (van't Hoff equation) tell that the side to which an equilibrium is shifted by varying temperature is *only* governed by the sign of ΔH. We thank Prof. Gideon Fraenkel for bringing this to our attention.

(21) Seebach, D.; Hässig, R.; Gabriel, J. *Helv. Chim. Acta* **1983**, *66*, 308. Heinzer, J.; Oth, J. F. M.; Seebach, D. *Helv. Chim. Acta* **1985**, *68*, 1848.

(22) (a) Kutzelnigg, W. *Isr. J. Chem.* **1980**, *19*, 193. (b) Schindler, M.; Kutzelnigg, W. *J. Chem. Phys.* **1982**, *76*, 1919. (c) Kutzelnigg, W.; Schindler, M.; Fleischer, U. *NMR, Basic Principles and Progress*; Springer-Verlag: Berlin and New York, in press.

(23) Hydrocarbons: Schindler, M.; Kutzelnigg, W. *J. Am. Chem. Soc.* **1983**, *105*, 1360. Carbocations: (a) Schindler, M. *J. Am. Chem. Soc.* **1987**, *109*, 1020. (b) Bremer, M.; Schleyer, P. v. R.; Schötz, K.; Kausch, M.; Schindler, M. *Angew. Chem.* **1987**, *99*, 795; *Angew. Chem., Int. Ed. Engl.* **1987**, *26*, 761. (c) Schleyer, P. v. R.; Laidig, K. E.; Wiberg, K. B.; Saunders, M.; Schindler, M. *J. Am. Chem. Soc.* **1988**, *110*, 300. (d) Saunders, M.; Laidig, K. E.; Wiberg, K. B.; Schleyer, P. v. R. *J. Am. Chem. Soc.* **1988**, *110*, 7652. (e) Bremer, M.; Schleyer, P. v. R. *J. Am. Chem. Soc.* **1989**, *111*, 1147. Organolithium compounds: Bühl, M.; Schleyer, P. v. R.; Fleischer, U.; Hommes, N. v. E. *J. Am. Chem. Soc.*, in press. (g) Fleischer, U.; Schindler, M.; Kutzelnigg, W.; Bühl, M.; Hommes, N. v. E.; Scheleyer, P. v. R., to be published.

(24) The experimental ^{6}Li NMR spectra are not referenced to "naked" Li^+ but rather to 1 M LiBr in THF. Therein, lithium is likely to exist as $[Li(THF)_4]^+$. However, according to IGLO, solvation of Li^+ with H_2O (as a model for THF) results only in minor changes for σ(Li): $\sigma(Li^+)$ = 95.4 ppm; $\sigma([Li(H_2O)_4]^+)$ = 96.8 ppm: Bühl, M.; Schleyer, P. v. R. Unpublished results.

(25) Bauer, W.; Seebach, D. *Helv. Chim. Acta* **1984**, *67*, 1972.

THF solution at low temperatures where both species can be observed separately.

A first hint comes from the ^{1}H NMR spectrum (cf. Figures 3 and 4). Thus, the resonance of H10(syn) of the dimer appears appreciably downfield from the corresponding line of the monomer ($\Delta\delta$ = +0.30 ppm). On the other hand, the signal of H8,9(endo) of the dimer appears only slightly upfielded from that of the monomer ($\Delta\delta$ = −0.13 ppm). This behavior is compatible with a bis exo dimer structure **6**: H10(syn) should experience the intraaggregate ring current of the second attached isodiCp moiety. In contrast to lithium, which lies in the shielding cone of each Cp ring,[26] H10(syn) is located at the periphery and is thus shifted downfield. If the bis endo dimer **7** were present, the opposite behavior might be expected (downfield shift of H8,9(endo) in the sandwich dimer as compared to the monomer).

In order to confirm this stereochemical assignment further, we recorded a ROESY (rotating frame nuclear Overhauser spectroscopy) spectrum[6,27] of **1** in THF at −100 °C. Compared to conventional 2D NOESY[6,28] spectra, ROESY offers several advantages. The sign and the magnitude of the homonuclear NOE is a function of the molecular correlation time and thus of temperature. At very low temperatures, negative NOEs are usually found even for small molecules. Therefore, in a NOESY spectrum recorded at low temperatures, NOE cross peaks appear with the same phase as exchange cross peaks and cannot be distinguished from each other.[4] This is avoided by ROESY where the phase of the NOE cross peaks is always opposite to that of the exchange cross peaks.[4]

Figure 6a shows the ROESY contour plot of **1** in THF. Parts b–e of Figure 6 show selected f_1 traces (columns) of the same spectrum. Even at −100 °C, the exchange rate between the two aggregates is considerable, resulting in intense exchange cross peaks at the corresponding positions. If the bis exo dimer **6** were prevailing in THF solution at −100 °C, a NOE can be expected between H10(syn) of one monomer subunit and H3,4,5 of the opposing subunit. Clearly, this is found in Figure 6b (indicated by an arrow). To confirm that this effect is not due to an *intra*unit NOE, the f_1 trace of H10(syn) of the monomer signal was taken (Figure 6c): no cross peak is visible at the corresponding position (arrow). In agreement with the experimental results, MNDO (see below) finds the shortest *inter*unit distance H10(syn)–H3,4,5 in the bis exo dimer to be 3.37 Å whereas the shortest *intra*unit distance between these positions is 4.73 Å (structure **30** in Figure 10).

In order to further rule out the bis endo dimer **7**, the f_1 traces of the ROESY spectrum for H8,9(endo) were taken both for the monomer and for the dimer (Figure 6d and e). In each one of these a small *intra*unit NOE between H8,9(endo) and H3,5 is visible. This can be rationalized by the smaller *intra*unit distance of H8,9(endo)–H3,5 (MNDO, 3.70 Å) as compared to H10(syn)–H3,5 (MNDO, 4.70 Å, structure **30** in Figure 11). If a bis endo dimer **7** were present, a much larger NOE should be observed for this species [MNDO, shortest *inter*unit distance H8,9(endo)–H3,5 = 2.98 Å in the bis endo dimer structure **31**].

That an exo monomer **4**–bis exo dimer **6** equilibrium is present also is deduced from comparison with known ^{1}H NMR chemical shifts.[2] In the exo titanocene derivative **18**, H3,5 resonate at 6.15

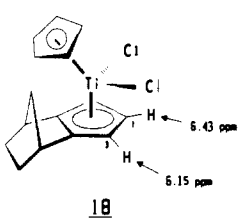

18

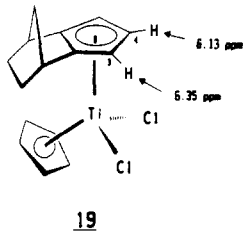

19

ppm whereas H4 absorbs at 6.43 ppm; i.e., H4 appears downfield from H3,5. This order is reversed in the endo isomer **19**; therein, H3,5 appear at 6.35 ppm while H4 is found at 6.13 ppm. Clearly, in our case, in both the monomer and the dimer of **1** H4 resonates *downfield* from H3,5 (cf. Figure 3 and Table I). By analogy, both species observed should be exo isomers.

The most direct evidence for lithium location in both the monomer and the dimer of **1** in THF comes from two-dimensional ^{6}Li,^{1}H heteronuclear Overhauser effect spectroscopy (HOESY). This method was recently introduced by our group for the detection of short (ca. <3.5 Å) ^{6}Li–^{1}H distances in lithioorganic compounds.[8,29] Thus, in a HOESY contour plot cross peaks indicate nearby ^{6}Li and ^{1}H nuclei.

Inherently, the ^{6}Li,^{1}H NOESY pulse sequence involves a mixing period, τ_m, which should be set to the order of the spin–lattice relaxation times (T_1) of the involved nuclei.[30] Optimum values

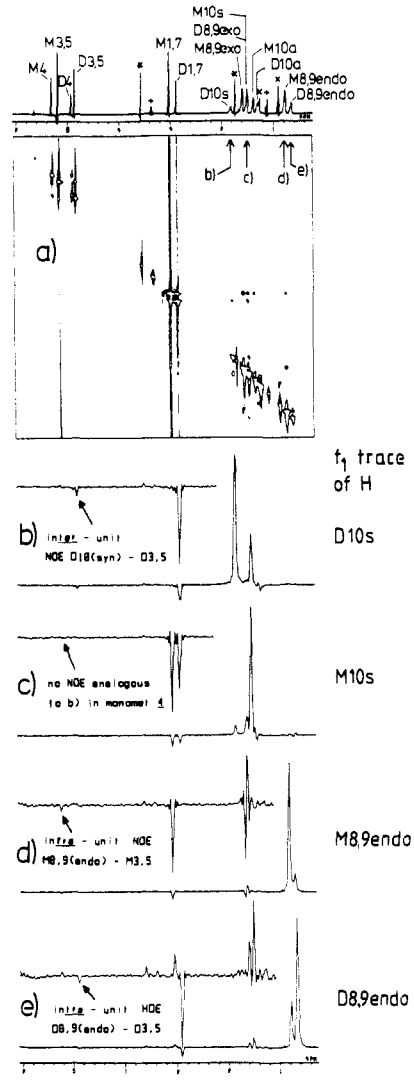

Figure 6. (a) ROESY contour plot of Li–isodiCp **1** in THF-d_8, 0.68 M, at −100 °C. Mixing time, 70 ms. Negative contours (indicating NOE cross peaks) are drawn as filled circles, positive contours (diagonal peaks and exchange cross peaks) are displayed as open circles. M, monomer **4**; D, dimer **6**; *, solvent signal (THF-d_8); x, hexane; +, diethyl ether. (b)–(e) Selected f_1 traces from (a) taken at the arrows indicated in the one-dimensional spectrum.

(26) Haigh, C. W.; Mallion, R. B. *Org. Magn. Reson.* **1972**, *4*, 203.
(27) Bothner-By, A. A.; Stephens, R. L.; Lee, J.-M.; Warren, C. D.; Jeanloz, R. W. *J. Am. Chem. Soc.* **1984**, *106*, 811. Bax, A.; Davis, D. *J. Magn. Reson.* **1985**, *63*, 207.
(28) Jeener, J.; Meier, B. H.; Bachmann, P.; Ernst, R. R. *J. Chem. Phys.* **1979**, *71*, 4546.
(29) Bauer, W.; Müller, G.; Pi, R.; Schleyer, P. v. R. *Angew. Chem.*, **1986**, *98*, 1130; *Angew. Chem., Int. Ed. Engl.* **1986**, *25*, 1103. Bauer, W.; Clark, T.; Schleyer, P. v. R.; *J. Am. Chem. Soc.* **1987**, *109*, 970. Bauer, W.; Winchester, W. R.; Schleyer, P. v. R. *Organometallics* **1987**, *6*, 2371. Bauer, W.; Klusener, P. A. A.; Harder, S.; Kanters, J. A.; Duisenberg, J. M.; Brandsma, L.; Schleyer, P. v. R. *Organometallics* **1988**, *7*, 552. Bauer, W.; Schleyer, P. v. R.; *Magn. Reson. Chem.* **1988**, *26*, 827.

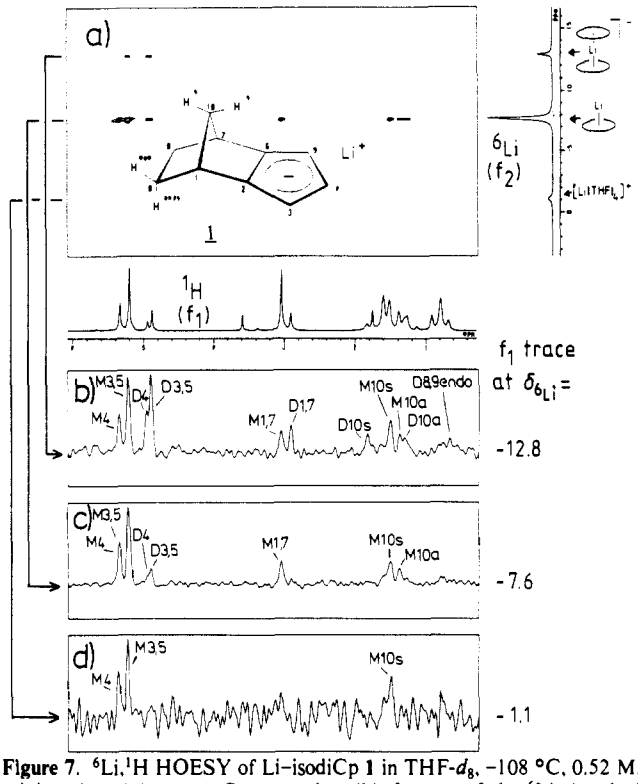

Figure 7. ^{6}Li,^{1}H HOESY of Li-isodiCp **1** in THF-d_8, −108 °C, 0.52 M, mixing time 1.1 s. (a) Contour plot; (b) f_1 trace of the ^{6}Li signal of "sandwiched" Li in dimer **6**; (c) f_1 trace of the ^{6}Li signal of monomer **4**; (d) f_1 trace of $[^6Li(THF\text{-}d_8)_4]^+$–"external" lithium.

for τ_m in ^{6}Li,^{1}H HOESY experiments were found to be ca. 2.0 s.[29] However, in the case of **1**, one has to cope with considerable interaggregate monomer–dimer exchange even at the lowest accessible temperatures when using this long mixing period. It will be shown below that the monomer–dimer exchange rate is in the order of seconds for **1** under these circumstances. This may lead to cross peaks appearing at positions in the f_1 domain that are not directly involved in the NOE buildup. Thus, in order to restrict the heteronuclear NOE mainly to the nuclei directly involved and to reduce transferred NOE (TRNOE),[4] we used a smaller mixing time of 1.1 s. However, this resulted in poorer signal to noise ratios.

When applied to **1** in THF at −108 °C, the spectrum shown in Figure 7 is obtained. The appropriate cross peaks can be visualized best by looking at the f_1 traces of the three lithium signals (Figure 7b–e). The top slice (Figure 7b) refers to the dimer, i.e., to ^{6}Li sandwiched between two monomer units. Intense cross peaks are detected that involve the ^{1}H signals H3,4,5 (Cp ring) and H1,7 (bridgeheads). This indicates close proximity of lithium to these positions. However, neither the bis exo nor the bis endo species are indicated by these cross peaks. Additionally, at higher field a cross peak to H10(syn) is visible. This indicates the presence of the proposed bis exo dimer **6**.

Further cross peaks in Figure 7b appear between ^{6}Li and H10(anti) and (albeit weak) between ^{6}Li and H8,9(endo). At first glance, this seems to conflict with the proposed bis exo dimer. However, it will be shown below (MNDO section) that the cross peak between Li and H8,9(endo) is likely to be due to a transferred NOE arising from an "external" lithium in structure **34** or an analogue.

The second "artificial" cross peak in Figure 7b that involves H10(anti) cannot be rationalized by close lithium–hydrogen contacts in either species. Rather, this might be due to strong coupling between H10(syn) and H10(anti). Thus, the ^{6}Li nucleus is the X part of an ABX spin system with $J_{AX} = J_{BX} \approx 0$. In these cases NOEs are also found to the remote but strongly coupled H10(anti) nucleus. Analogous strong coupling effects in HOESY had been observed earlier for ^{1}H and ^{13}C nuclei by Kövér and Batta in oligosaccharides.[31] The underlying theory of this phenomenon is discussed in ref 4.

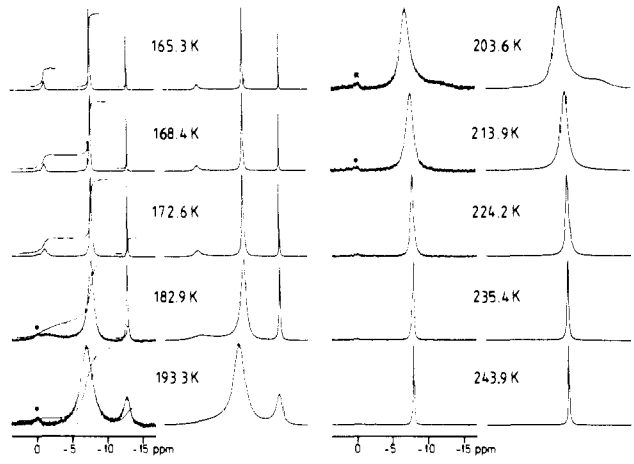

Figure 8. Temperature-dependent experimental (left) and calculated (right) ^{6}Li NMR spectra of Li-isodiCp **1** in THF-d_8, 0.8 M. *, impurity signal.

The f_1 trace shown in Figure 7c is taken at $\delta_{^6Li} = -7.6$ ppm and involves the ^{6}Li signal of the monomer. Cross peaks are visible to H1,3,4,5,7, as was the case for the dimer. Again, neither an exo nor an endo monomer is indicated. However, an intense cross peak between ^{6}Li and H10(syn) clearly suggests the monomer to be a species **4** with lithium at the *exo* face.

The third ^{6}Li trace (Figure 7d) refers to the lithium counterion of the dimer sandwich anion. If this actually was $[Li(THF\text{-}d_8)_4]^+$, there should be no cross peaks at all in this trace as considerable spatial separation from the anion can be assumed. Clearly, this is not found. However, we will show below that there is rapid exchange between this lithium site and the site of lithium located at the monomer. As the involved exchange rate is in the order of 100 s^{-1} at −108 °C, the cross peak intensity ratios within this f_1 trace should be identical with those of the trace of Figure 7c. Only the low intensity of the ^{6}Li signal itself would then account for the poorer overall signal to noise ratio for this f_1 trace.

On the other hand this lithium site might as well involve a cation that is located at the periphery of the dimer anion sandwich (stacked CIP). If so, cross peaks involving the anion moiety should be observed. Presumably, we deal with a rapid solvent-separated ion pair (SSIP)–CIP equilibrium of the dimer as is outlined below.

In summary, there are several independent indications that **1** is present as an exo monomer **4**–bis exo dimer **6** equilibrium mixture in THF at ca. −100 °C.

Line-Shape Analysis

The temperature-dependent ^{6}Li NMR spectra of **1** in THF-d_8 are shown in Figure 8. In going from −108 to −90 °C, the −1.10 and −7.64 ppm signals broaden whereas the −12.78 ppm peak still remains sharp. At the coalescence point for the −1.10 and the

(30) Kövér, K. E.; Batta, G. *J. Magn. Reson.* **1986**, *69*, 344. Kövér, K. E.; Batta, G. *Prog. Nucl. Magn. Reson. Spectrosc.* **1987**, *19*, 223.

(31) (a) Kövér, K. E.; Batta, G. *J. Magn. Reson.* **1987**, *74*, 397. (b) We would like to emphasize that the explanation concerning the reason for the appearance of positive cross peaks for H10(anti) in Figure 7b and c is only tentative. A reviewer has pointed out that the strong coupling condition is not met, at least for H10(anti) and H10(syn) of the dimer of Figure 7b. Since "the Li-H(s)-H(a) system must be very nearly linear, one would expect *negative* cross peaks in the phase-sensitive HOESY as can be seen by referring to Figures 6–11 in ref 4". However, the claimed three-spin system is not linear (cf. the structures in Figures 10 and 11). Furthermore, the conditions described in ref 4, Chapter 6.3, refer to an ABX spin system under irradiation of the X nucleus, whereas in our system A and B are the irradiated nuclei. In addition, Figure 6.11 in ref 4 refers to a *steady-state* NOE whereas in our case we deal with a *transient* NOE. Our situation much more resembles that described in ref 31a, where the strong coupling parameters are comparable to those of our system. Therein, clearly *positive* NOE cross peaks arise from strong coupling effects. We currently apply the methods proposed in ref 31a to our system in order to evaluate these effects. Nevertheless, we are very much indepted to the reviewer for this stimulating comment.

Scheme II

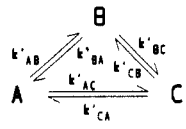

Scheme III

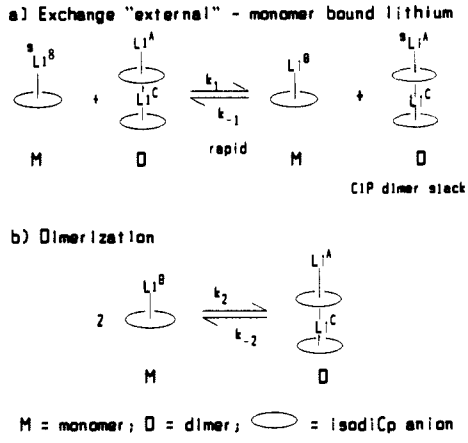

−7.64 ppm peak (ca. −85 °C), the signal at −12.78 ppm also broadens. Upon further warming, coalescence of the −12.78 ppm peak with the already coalesced signal is observed at ca. −65 °C. At temperatures above ca. −50 °C, a single sharp signal is found.

In order to evaluate the rate constants, a line-shape analysis was carried out with the program DNMR3.[32] For convenience, we assign the three lithium peaks as A (−1.10 ppm), B (−7.64 ppm), and C (−12.78 ppm; see Figure 8). Likewise, these letters denote the species involved, i.e., A = $[Li(THF\text{-}d_8)_4]^+$ (or, alternatively, contact ion paired "external" lithium), B = lithium in monomer **4**, and C = lithium sandwiched in dimer **6**. For simplicity, we assume in the following that site A involves exclusively contact ion paired lithium, analogous, e.g., to the MNDO structures **32–34** (Figure 11).

The spectra suggest that two independent kinetic processes take place: the first is the relatively rapid exchange A ⇌ B, i.e., the exchange of "external" lithium with monomer-bound lithium. The second slower process involves exchange of C with the averaged signal of A and B, i.e., exchange between the "sandwiched" lithium and the lithium that is rapidly fluctuating between the periphery of the dimer CIP and the monomer. For a three-site exchange we can write the general kinetic Scheme II, where k'_{ij} denotes the pseudo-first-order rate constant for the transfer of magnetization from spin i to spin j.

We calculated the line shapes by assuming $k'_{AC} = k'_{CA} = 0$ (i.e., with no direct exchange between spins A and C). A reasonable fit with the experimental spectra is obtained if the two independent rate constants k'_{AB} and k'_{BC} are properly adjusted. Note that the rate constants k'_{BA} and k'_{CB} of the reverse reactions are correlated with the former ones by the populations of A, B, and C. Introducing appreciable rates for k'_{AC} gave poor fits with the experimental line shapes due to early broadening of line C. Likewise, an attempt to simulate the line shapes by using $k'_{BC} = 0$ and $k'_{AC} > 0$ gave no reasonable picture.

Next, we have to relate the obtained NMR rates to an adequate mechanism. Obviously, no exchange between A and C takes place; i.e., there is no direct interchange of "external" and "sandwiched" lithium in a CIP dimer stack. Whenever two monomers M (Li type B) aggregate to give a dimer D, lithium species of type A and C are formed simultaneously. However, there is an additional exchange process, which involves the "external" lithium of the CIP dimer stack (site A) and the monomer-bound lithium (site B). The two assumed exchange processes are depicted in Scheme III.

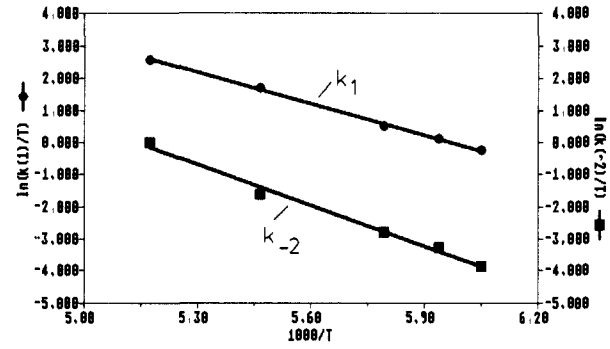

Figure 9. Eyring plot [ln (k/T) vs $1/T$] of the kinetic data extracted from Figure 8 (see Table IV). Only the low temperature data up to −80 °C have been used (see text).

Under steady-state conditions we can write for the dimerization process b

$$-d[M]/dt = k_2[M]^2 - k_{-2}[D] = 0 \quad (2)$$

and thus

$$k_2[M]^2 = k_{-2}[D] \quad (3)$$

This is related to the transfer of magnetization from spin B to spin C by eq 4:

$$k'_{BC} = k_2[M] = k_{-2}[D]/[M] \quad (4)$$

The absolute concentrations of the monomer [M] and the dimer [D] can be derived from the known overall concentration and the integral ratios of the ^{6}Li NMR spectra of Figure 8. Thus, by use of eq 4, k_{-2} can be calculated from the measured rate constant k'_{BC}.

The exchange process a (Scheme III) is related to k'_{BA} by eq 5.

$$k'_{BA} = k_1[D] + k_2[M] \quad (5)$$

This is due to the following. For spin B (monomer) there are two different ways to turn into spin A ("external" lithium in the dimer CIP stack): either by a dimerization process (b) (k_2) or by mutual exchange (a) (k_1). Both processes are bimolecular.

As the exchange process a (Scheme III) is degenerate it follows

$$k_1 = k_{-1} \quad (6)$$

Thus, eq 5 may alternatively be written as eq 7.

$$k'_{AB} = k_1[M] + k_{-2} \quad (7)$$

By use of k_{-2} evaluated above k_1 is given by

$$k_1 = (k'_{AB} - k_{-2})/[M] \quad (8)$$

The absolute concentrations [A], [B], and [C] are extractable from the ^{6}Li NMR integrals only in the region of slow chemical exchange (up to −80 °C). As mentioned earlier, there is no significant change of the relative line intensities of A, B, and C between −108 and −80 °C. For higher temperatures the intensity ratios have to be extrapolated. Clearly, since at high temperatures (+25 °C) the equilibrium is apparently shifted to the side of monomer B (**4**), systematic errors would occur. Thus, for the evaluation of the kinetic parameters $\Delta H^{\ddagger}$ and $\Delta S^{\ddagger}$ we have not employed the spectra above −80 °C. Hence, only a limited data set was available for the Eyring plot[33] shown in Figure 9. The full list of rate constants used for the simulation shown in Figure 8 is given in Table IV.

The Eyring activation parameters, obtained from the program ACTPAR,[34] are as follows:

(32) Kleier, D. A.; Binsch, G. DNMR3. *Quantum Chemistry Program Exchange* (*QCPE*) **1969**, *No. 163.*

(33) Sandström, J.; *Dynamic NMR Spectroscopy*; Academic Press: London, 1982.

for k_1 (exchange of "external" Li with monomer bound Li)

$$\Delta H^{\ddagger} = 6.5 \pm 0.2 \text{ kcal/mol} \quad (9)$$

$$\Delta S^{\ddagger} = -8.4 \pm 0.9 \text{ eu} \quad (10)$$

and

for k_{-2} (exchange "sandwiched" → monomer-bound Li)

$$\Delta H^{\ddagger} = 8.6 \pm 0.5 \text{ kcal/mol} \quad (11)$$

$$\Delta S^{\ddagger} = -3.2 \pm 2.7 \text{ eu} \quad (12)$$

Unfortunately, due to the "early" coalescence, no reliable thermodynamic data $\Delta H°$ and $\Delta S°$ for the dimer **6**–monomer **4** equilibrium could be derived from a van't Hoff plot. Therefore, discussion of the kinetic parameters is of limited value.

The negative activation entropy for the exchange "external" Li–monomer-bound Li indicates that the transition state of this process is highly ordered. Thus, it is unlikely that free ions are involved. The lower activation entropy of the second exchange process "sandwiched" Li–monomer-bound Li (disaggregation of the dimer) might indicate that in the transition state the two monomers are already "preformed". This agrees with the assumption of a dimer stack CIP being present in THF-d_8 solution, analogous to, e.g., structures **32**–**34** in Figure 11 (with THF-d_8 instead of water).

However, in the ^1H and ^{13}C NMR spectra of **1** in THF-d_8, only *one* set of signals is observed for the dimer. Clearly, this is incompatible with a *static* CIP dimer stack (cf. Scheme III). Instead, there must be rapid exchange of the "external" lithium between the "upper" and the "lower" side of the sandwich anion. Presumably, this involves a solvent-separated ion pair (SSIP) where the "external" lithium is converted to $[Li(THF\text{-}d_8)_4]^+$ (eq 13, where R = triple ion sandwich; cf. **6**).

$$RLi(THF\text{-}d_8)_3 + THF\text{-}d_8 \rightleftharpoons R^- + [Li(THF\text{-}d_8)_4]^+ \quad (13)$$

An indication for this additional exchange process comes from the concentration-dependent ^6Li NMR spectra (Figure 5): whereas the signals of monomer-bound Li ($\delta = -7.64$ ppm) and of "sandwiched" Li ($\delta = -12.78$ ppm) remain constant, the signal of "external" Li is slightly shifted to lower field when the concentration is decreased.

When the above kinetic data are calculated with the assumption of a SSIP **6** being present exclusively as the dimer species, there is no significant change in the results. Therefore, in the following we use "$[Li(THF\text{-}d_8)_4]^+$" and "external Li" with the same meaning. Likewise, formula **6** is used as representation of the dimer, irrespective of its actual nature (CIP or SSIP).

Interestingly, the temperature-dependent ^7Li signals described by Fraenkel[9] have shapes similar to those given by **1**. However, his exchange rates are considerably smaller than those indicated for our system.

The line widths of the ^6Li signals at −95 °C and hence the exchange rates decrease when the overall concentration of **1** is reduced (Table V). This is reasonable as the observed rate constants k'_{AB}, k'_{BC}, etc. depend on the concentrations of the monomer and the dimer (see eqs 2–9). Similar observations have been made, e.g., by Seebach for the exchange of dimeric and tetrameric *n*-BuLi.[21] Clearly, in order to elucidate further the underlying exchange mechanisms, a line-shape analysis of the concentration-dependent ^6Li NMR spectra would be adequate.

MNDO Calculations

Semiempirical MNDO calculations[35] are established to be a valuable tool for structure analysis of organolithium compounds.[36]

Table IV. Rate Constants and Absolute Concentrations Used for the Simulated Line Shapes of Figure 8[a]

T	$10^3/T$	[M]	[D]	k'_{AB}	k'_{BC}	k_{-2}	k_1
165.3	6.050	0.60	0.14	80	0.8	3.4	128
168.4	5.938	0.60	0.14	120	1.5	6.4	189
172.6	5.794	0.59	0.14	180	2.5	10.5	287
182.9	5.467	0.59	0.14	630	8.6	36	1006
193.3	5.173	0.59	0.14	1700	45.0	190	2560
203.6	4.912			5000	185		
213.9	4.675			20000	900		
224.2	4.460			70000	2000		
235.4	4.248			300000	4000		
243.9	4.100			800000	6000		

[a] T, K; M, monomer; D, dimer; [M] and [D] in mol/L; k'_{AB}, k'_{BC}, and k_{-2} in s^{-1}; k_1 in L/(mol s).

Table V. Line Width of the ^6Li Signal of Monomer **4** ($\delta = -7.64$ ppm) at Different Concentrations (THF-d_8, −95 °C)

M	Hz	M	Hz
0.86	30	0.18	10
0.63	25	0.05	3
0.24	13		

A number of structures related to monomeric and dimeric **1** were calculated in order to rationalize our experimental results. These are shown in Figures 10 and 11. Water was used as a model for the THF ligand.

Except for the solvent-separated ion pairs **29**, **37**, and **45** all structures were optimized by using the MNDO keyword PRECISE. In addition, the MNDO heats of formation of Li^+, of $[Li(H_2O)_4]^+$, and of H_2O are given in Figure 10.[37]

For the monomer, contact ion pairs with zero to four ligands were calculated (**21**–**28**). Of these, the exo lithio isomers are considerably more stable than their endo counterparts. This agrees nicely with the NMR findings: e.g., for the two-ligand CIPs **25** and **26** the endo vs exo energy difference is 1.4 kcal/mol, and the three-ligand CIPs **27** and **28** differ by 2.7 kcal/mol. Thus, if an exo/endo equilibrium were present in solution, it should be largely on the exo side.

Of the four alternative exo monomers with zero to three ligands (**21**, **23**, **25**, and **27**), the three-ligand exo monomer is favored (eqs 14–16).

$$\underset{18.9}{\mathbf{21}} + \underset{-60.9}{H_2O} \rightleftharpoons \underset{-59.9}{\mathbf{23}} \quad \Delta H = -17.9 \text{ kcal/mol} \quad (14)$$

$$\underset{-59.9}{\mathbf{23}} + \underset{-60.9}{H_2O} \rightleftharpoons \underset{-128.1}{\mathbf{25}} \quad \Delta H = -7.3 \text{ kcal/mol} \quad (15)$$

$$\underset{-128.1}{\mathbf{25}} + \underset{-60.9}{H_2O} \rightleftharpoons \underset{-197.1}{\mathbf{27}} \quad \Delta H = -2.1 \text{ kcal/mol} \quad (16)$$

This is interesting in the context of Jutzi's[38] solid-state structure of a lithium cyclopentadienide derivative **47**. The η^3 ligand pentamethyldiethylenetriamine (PMDTA) is bound only in a η^2 fashion to lithium. Furthermore, structures **48** and **49** with only one monodentate ligand bound to lithium (THF[39] and quinu-

(34) Binsch, G.; Kessler, H. *Angew. Chem.* **1980**, *92*, 445; *Angew. Chem., Int. Ed. Engl.* **1980**, *19*, 411.
(35) Dewar, M. J. S.; Thiel, W. *J. Am. Chem. Soc.* **1977**, *99*, 4899, 4907. Li parametrization: Thiel, W.; Clark, T., unpublished.

(36) Bausch, J. W.; Gregory, P. S.; Olah, G. A.; Prakasch, G. K.; Schleyer, P. v. R.; Segal, G. A. *J. Am. Chem. Soc.* **1989**, *111*, 3633. McKee, M. L. *J. Am. Chem. Soc.* **1987**, *109*, 559. Hacker, R.; Kaufmann, E.; Schleyer, P. v. R.; Mahdi, W.; Dietrich, H. *Chem. Ber.* **1987**, *120*, 1533. Hacker, R.; Schleyer, P. v. R.; Reber, G.; Müller, G.; Brandsma, L. *J. Organomet. Chem.* **1986**, *316*, C4. Wilhelm, D.; Clark, T.; Schleyer, P. v. R.; Dietrich, H.; Mahdi, W. *J. Organomet. Chem.* **1985**, *280*, C6. Schleyer, P. v. R.; Hacker, R.; Dietrich, H.; Mahdi, W. *Chem. Commun.* **1985**, 622. Neugebauer, W.; Geiger, G. A. P.; Kos, A. J.; Stezowski, J. J.; Schleyer, P. v. R. *Chem. Ber.* **1985**, *118*, 1504. Stezowski, J. J.; Hoier, H.; Wilhelm, D.; Clark, T.; Schleyer, P. v. R. *Chem. Commun.* **1985**, 1263. Dietrich, H.; Mahdi, W.; Wilhelm, D.; Clark, T.; Schleyer, P. v. R. *Angew. Chem.* **1984**, *96*, 623; *Angew. Chem., Int. Ed. Engl.* **1984**, *23*, 621. Boche, G.; Decher, G.; Etzrodt, H.; Dietrich, H.; Mahdi, W.; Kos, A. J.; Schleyer, P. v. R. *Chem. Commun.* **1984**, 1493.
(37) Kaufmann, E.; Gose, J.; Schleyer, P. v. R. *Organometallics* **1989**, *8*, 2577.
(38) Jutzi, P.; Schlüter, E.; Krüger, C.; Pohl, S. *Angew. Chem.* **1983**, *95*, 1015; *Angew. Chem., Int. Ed. Engl.* **1983**, *22*, 994.
(39) Jutzi, P.; Leffers, W.; Pohl, S.; Saak, W. *Chem. Ber.* **1989**, *122*, 1449.

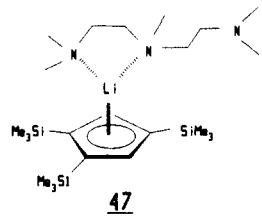

47

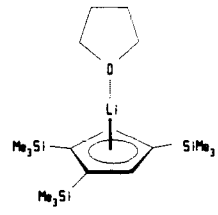

48

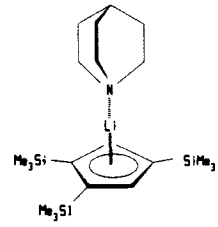

49

clidine[40]) are found in the crystal state. This may be due to steric reasons and might reflect the oversimplifications of modeling the ligands by the sterically less demanding water molecules.

The formation of SSIP **29** from the free ions is highly exothermic:

$$\underset{+28.8}{\mathbf{20}} + [Li(H_2O)_4]^+ \rightleftharpoons \underset{-218.2}{\mathbf{29}} \quad \Delta H = -58.6 \text{ kcal/mol} \quad (17)$$
$$\qquad\qquad -188.4$$

Likewise, the formation of CIP **27** from the SSIP **29** is an exothermic process:

$$\underset{-218.2}{\mathbf{29}} \rightleftharpoons \underset{-191.1}{\mathbf{27}} + \underset{-60.9}{H_2O} \quad \Delta H = -33.8 \text{ kcal/mol} \quad (18)$$

When the geometry optimization of SSIP **29** is attempted with the MNDO keyword PRECISE, the lithium is "captured" by the Cp ring to give a CIP where Li is "bound" to C4 ($\Delta H°_f = -241.3$ kcal/mol). Thus, **29** is not a true minimum. In fact, a frequency calculation revealed four negative eigenvalues, but these were small in magnitude. The transition vectors correspond to rotations of the H_2O ligands. Thus, **29** is not a true transition state. Instead, it represents a stationary point in a local area of the potential energy surface, which must be quite flat.

The MNDO calculated dimers of **1** subdivide into two different rotamers. Structures **30–37** involve Cp rings with the edges fused to the norbornyl residues at "opposite" positions. By contrast, in structures **38–45** the fused Cp edges are "adjacent" with respect to a projection along the longitudinal Cp–Li–Cp axis.

In the former series, the bis exo triple anion sandwich **30** is 4.0 kcal/mol more stable than its bis endo counterpart **31**. This preference agrees with the above experimental results of a bis exo dimer being present in THF-d_8 at low temperatures.

From simple symmetry considerations it might be expected that the rotamers with C_1 symmetry might be most stable. These would involve "staggered" Cp rings and exactly opposite norbornyl residues (not shown in Figure 10). However, both the exo and the endo dimer sandwich anions **30** and **31** (with eclipsed Cp rings) are each 0.3 kcal/mol more stable.

A frequency calculation on the staggered bis exo isomer **30** revealed a small negative eigenvalues (−12.8 cm^{-1}). Thus, rotation of the two subunits around the Cp–Li–Cp axis, at least to a limited extent, is essentially free. The slight preference of the eclipsed isomers is probably due to nonbonded interactions between the two anion subunits.

Clearly, a more detailed analysis of the dimer would involve the counterion. As for the monomer, the formation of SSIP **37** from free ion **30** and $[Li(H_2O)_4]^+$ is calculated to be strongly exothermic.

$$\underset{-7.7}{\mathbf{30}} + [Li(H_2O)_4]^+ \rightleftharpoons \underset{-242.3}{\mathbf{37}} \quad \Delta H = -46.2 \text{ kcal/mol} \quad (19)$$
$$\qquad\qquad -188.4$$

(40) Jutzi, P.; Schlüter, E.; Pohl, S.; Saak, W. *Chem. Ber.* **1985**, *118*, 1959.

Of the different possible isomers for a neutral stacked CIP dimer with "opposite" norbornyl moieties structures **32–36** were calculated. These differ in the number of the attached ligands (**32–34**), in the orientation of the "peripheral" lithium cation (**34** and **35**), and in the exo/endo face orientation toward the central lithium cation (**34** and **36**).

By analogy with the monomer, the formation of the dimer CIP **34** from SSIP **37** is strongly exothermic.

$$\underset{-242.3}{\mathbf{37}} \rightleftharpoons \underset{-198.0}{\mathbf{34}} + \underset{-60.9}{H_2O} \quad \Delta H = -16.6 \text{ kcal/mol} \quad (20)$$

Within the three differently solvated isomers the trisolvated species **34** proved to be most stable, as is indicated by eqs 21 and 22.

$$\underset{-66.5}{\mathbf{32}} + \underset{-60.9}{H_2O} \rightleftharpoons \underset{-135.9}{\mathbf{33}} \quad \Delta H = -8.5 \text{ kcal/mol} \quad (21)$$

$$\underset{-135.9}{\mathbf{33}} + \underset{-60.9}{H_2O} \rightleftharpoons \underset{-198.0}{\mathbf{34}} \quad \Delta H = -1.2 \text{ kcal/mol} \quad (22)$$

A trisolvated species **35**, which is similar to **34**, with however the peripheral lithium directing "inward", is much less stable.

Interestingly, whereas in the differently solvated exo monomers **21**, **23**, **25**, and **27** lithium is bound in a η^5 fashion, this is not found for the bis exo dimers. Whereas **32** and **33** behave similar to the monomers, the peripheral lithium cation in **34** switches to a η^1 position. This goes parallel with a structural change of the upper Cp ring in **34**: as is indicated by the bond lengths and bond orders involved, a cyclopentadiene geometry with localized double bonds is adopted.

Even more surprising, in structure **36**, which is the bis endo analogue of **34**, the peripheral lithium resumes its usual η^5 position. Thus, it is unlikely that steric repulsion is the reason for the η^1 geometry in **34**. Rather, favorable agostic Li–H interactions[29,41,42] in some of the calculated structures might explain this discrepancy.

Whereas the bis exo anion sandwich **30** was calculated to be significantly more stable than the bis endo isomer **31**, this is not found for the corresponding CIPs: actually, the trisolvated bis endo species **36** is 0.1 kcal/mol more stable than its bis exo analogue **34**. Again, this may be due to favorable Li–H interactions. However, as MNDO slightly overestimates both Li–C and Li–H interactions,[42] these small differences may not be significant.

The dimer structures **38–45** were calculated in Figure 11. These are analogous to structures **30–37**, however, with eclipsed Cp rings and with "adjacent" fused edges of the Cp rings (with respect to a projection along the Cp–Li–Cp axis). Experimentally, we have found a similar structure for the strongly related Fe(II) complex **46** in the crystal state.[43,44]

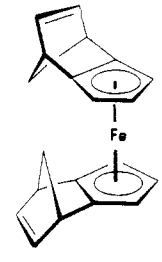

46

We have explained this geometry by "packing effects and/or weak intramolecular dipolar (London) interactions". Quite interestingly, all structures **38–45** are somewhat (0.1–0.2 kcal/mol) more stable than their analogues **30–37**. As MNDO calculations refer to the gaseous state, it seems that packing effects actually

(41) Brookhart, M.; Green, M. H. L. *J. Organomet. Chem.* **1983**, *250*, 395. Koga, N.; Obara, S.; Morokuma, K. *J. Am. Chem. Soc.* **1984**, *106*, 4625. Erker, G.; Frömberg, W.; Angermund, P.; Schlund, P.; Krüger, C. *Chem. Commun.* **1986**, 372.

(42) Kaufmann, E.; Raghavachari, K.; Reed, A.; Schleyer, P. v. R. *Organometallics* **1988**, *7*, 1597.

(43) Hsu, L.-Y.; Hathaway, S. J.; Paquette, L. A. *Tetrahedron Lett.* **1984**, *25*, 259.

(44) Paquette, L. A.; Schirch, P. F. T.; Hathaway, S. J.; Hsu, L.-Y.; Gallucci, J. C. *Organometallics* **1986**, *5*, 490.

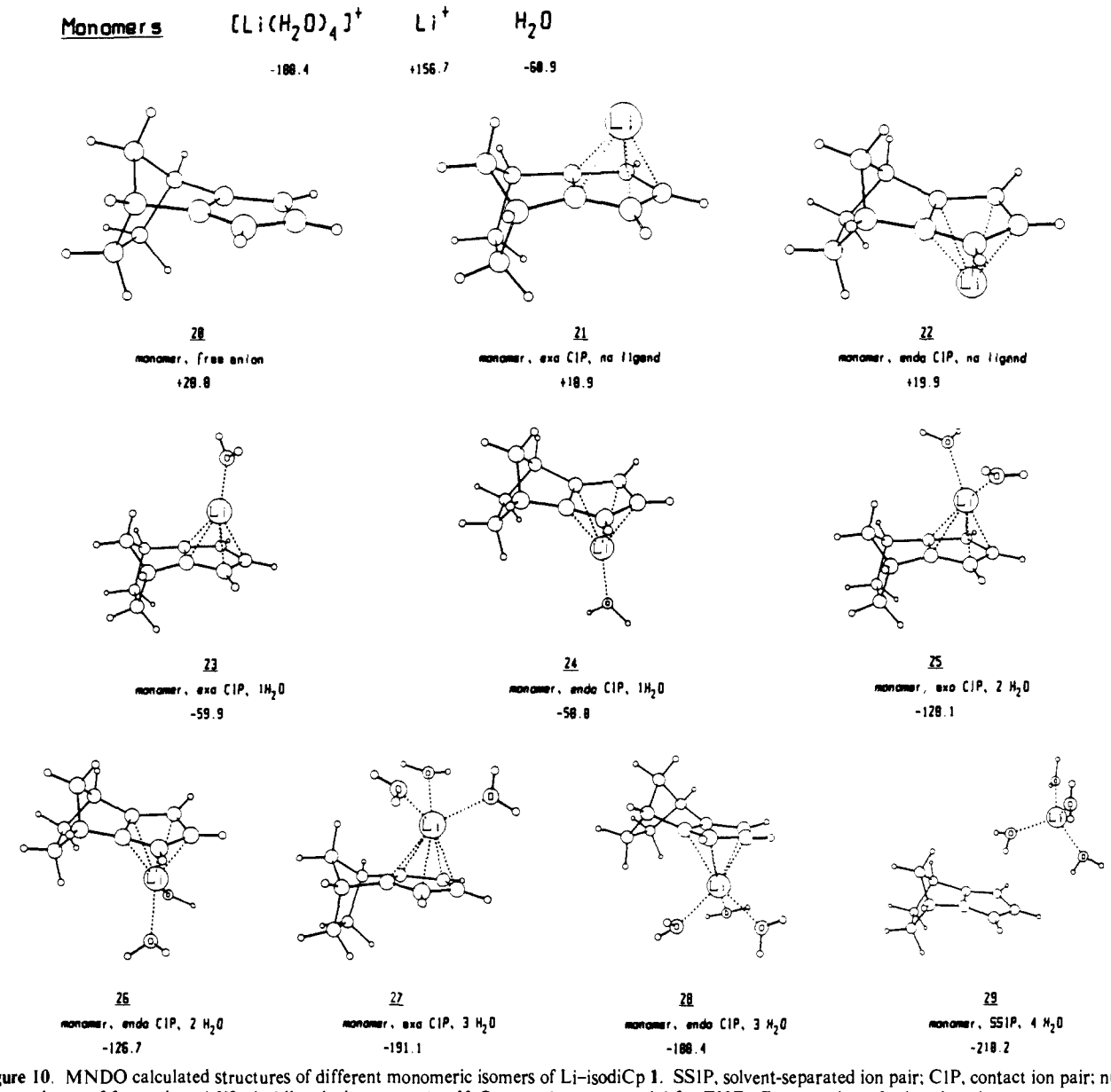

Figure 10. MNDO calculated structures of different monomeric isomers of Li-isodiCp **1**. SSIP, solvent-separated ion pair; CIP, contact ion pair; numbers refer to heats of formation, $\Delta H°_f$, in kilocalories per mole. H_2O was taken as a model for THF. For meaning of other descriptors, see text. Except for **29**, all structures were optimized by using the keyword PRECISE.

play no important role in the case of **46**. Instead, it is evident from the present MNDO studies that there is facile rotation of the Cp rings around the central axis, with a slight preference of the rotamers with "adjacent" fused Cp edges due to weak intramolecular forces.

If the MNDO calculations reflect the situation present in THF-d_8 solution, the CIP structures **32–34** as well as their rotamers **40–42** would account for the additional weak cross peak found in the HOESY experiment for the dimer (Figure 7b): the close contact between Li and H8,9(endo) can be explained by a transferred NOE. This might arise, e.g., from isomer **33** (with THF-d_8 instead of water), where the peripheral lithium is close to H8,9(endo).

As is found experimentally, the monomer–dimer equilibrium of **1** in THF probably is shifted toward the monomer at high temperatures; i.e., the reaction dimer → monomer must be endothermic. In contrast, eq 23 shows the MNDO calculated

$$\underset{-198.0}{\mathbf{34}} + \underset{3(-60.9)}{3H_2O} \rightleftharpoons \underset{2(-191.1)}{2\,\mathbf{27}} \quad \Delta H = -1.5 \text{ kcal/mol} \quad (23)$$

equilibrium to be silghtly exothermic. This decrepancy is probably due to the usage of the "simplified" ligand, water, instead of THF.

In summary, the MNDO results support the experimental findings of a fine balanced exo monomer **4**–bis exo dimer **6** equilibrium being present in THF-d_8 solution. In addition, MNDO confirms the assumption that the predominating structure of the dimer is a stacked CIP, e.g., similar to **34** as a model compound.

Mechanistic Proposal for the Stereoselectivity of the Electrophilic Attack

By combining the experimental and computational results we can provide a tentative answer to the initial question, i.e., why is **1** attacked from the endo side at low temperatures and from the exo side at high temperatures.

MNDO shows that CIPs are favored over SSIPs for both the monomer and the dimer of **1**. We believe that for both the monomer and the dimer CIPs of **1** are actually involved in the quench reactions.

At low temperatures in THF and at "normal" preparative concentrations an observable monomer–dimer equilibrium is present. For reasons not yet fully established the dimer appears to be the more reactive species. For the reaction of the bis exo dimer we propose that the electrophile [CH_3I, $(CH_3)_3SiCl$, $CpTiCl_3$] is first captured by the "peripheral" lithium of CIP **50** by replacing one THF ligand (Scheme IV).

This places the electrophile near the reactive site of the "anion", namely, the endo face of isodiCp. Subsequent bond formation

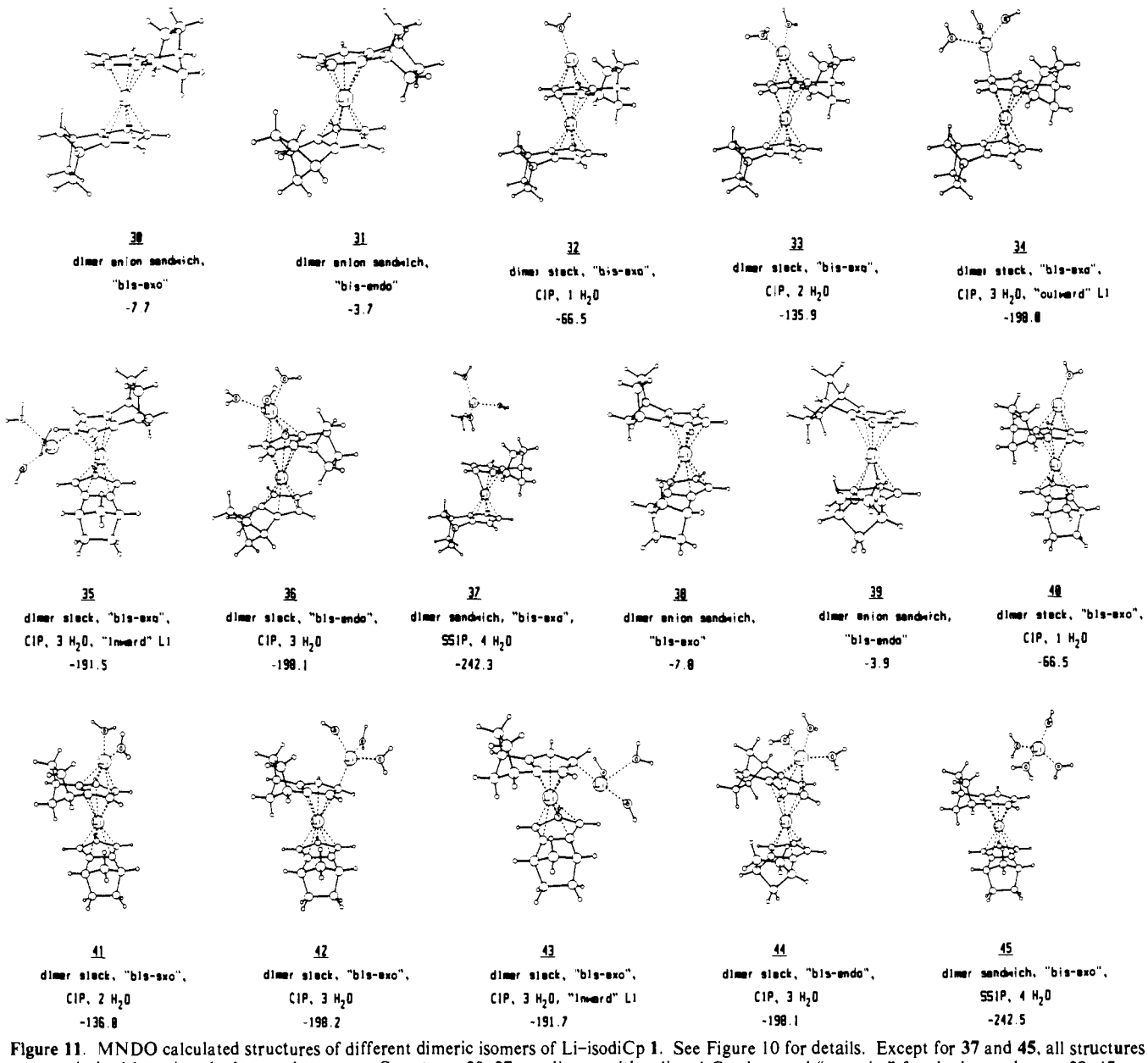

Figure 11. MNDO calculated structures of different dimeric isomers of Li-isodiCp **1**. See Figure 10 for details. Except for **37** and **45**, all structures were optimized by using the keyword PRECISE. Structures **30–37** are dimers with eclipsed Cp rings and "opposite" fused edges, whereas **38–45** are dimers with eclipsed Cp rings and "adjacent" fused edges.

and dissociation sets free endo **3**, the product observed at low temperatures.

At room temperature the nature of the prevailing species has not been established with certainty, but there are indications that only the exo monomer is present. By analogy with the proposed mechanism for the dimer (Scheme IV), association of the electrophile with lithium at the exo position of the monomer would lead to intermediate **54** (Scheme V). This would react further to the experimentally found exo product **2**.

Thus, the underlying mechanisms for the formation of the exo product **2** and the endo product **3** may be identical. The observed variations in stereoselectivity with temperature reflect the different degrees of aggregation that prevail at −80 °C (dimer–monomer equilibrium) and at +25 °C (exclusively monomer). Since the accessible sites differ, the electrophile is directed by preassociation with lithium to the endo face (dimers **6** and **50**) or to the exo face (monomer **4**).

Our observations and suggestions for the ortho lithiation of anisole[45] are similar.

(45) Bauer, W.; Schleyer, P. v. R. *J. Am. Chem. Soc.* **1989**, *111*, 7191.

Lithium Cyclopentadienide

The results obtained for **1** prompted us to reinvestigate the structure of lithium cyclopentadienide (CpLi) **56** in THF-d_8.

56

CpLi is one of the most widely used lithioorganic compounds. The crystal structure for unsubstituted CpLi has not been reported. However, in several substituted CpLi systems lithium is found experimentally to be bound centrally in a η^5 fashion to the Cp^- moiety.[46] CpLi is practically insoluble in nonpolar hydrocarbon solvents. The UV spectrum of **56** in diethyl ether was examined theoretically by Wagner.[47] The IR spectrum of **56** in THF was found to be consistent with a species of D_{5h}, C_{5v}, or D_{5d} symmetry.[48]

(46) Jutzi, P. *Adv. Organomet. Chem.* **1986**, *26*, 217.
(47) Wagner, B. O.; Ebel, H. F. *Tetrahedron* **1970**, *26*, 5155.
(48) Ford, W. T. *J. Organomet. Chem.* **1971**, *32*, 27.

Scheme IV

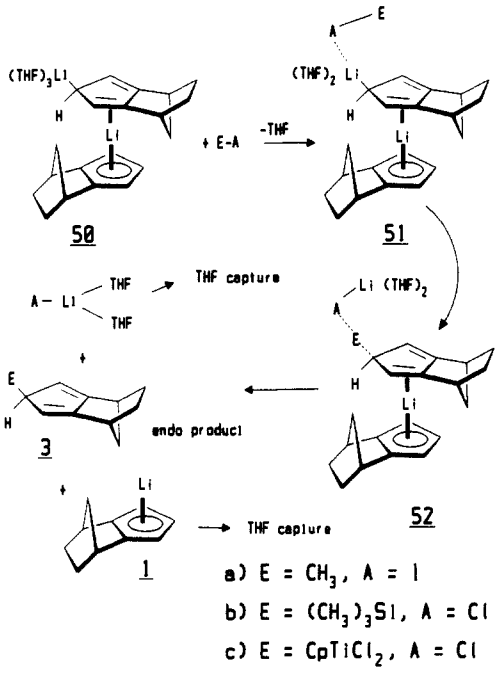

Scheme V

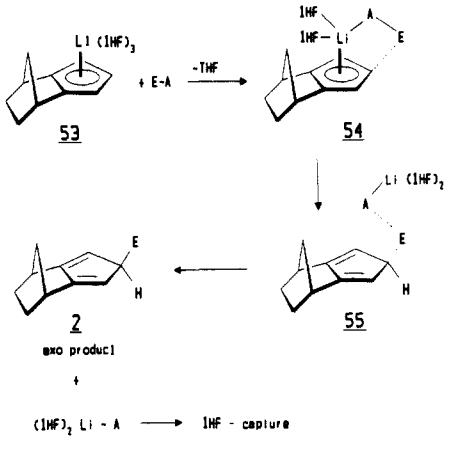

The ^{7}Li NMR chemical shift of **56** was reported by Cox to be −8.68, −8.37, −8.67, and −8.35 ppm in dioxane, THF, dimethoxyethane, and diglyme, respectively.[11] This unusual upfield shift was attributed to ring current phenomena as described above for **1**. However, in HMPA $\delta_{^7Li}$ was found to be 0.88 ppm, indicating a SSIP with $[Li(HMPA)_4]^+$ Cp^- structure. Since the ^{7}Li shifts of **56** in THF and DME do not depend on the concentration, Cox et al. concluded that "either aggregation effects are not important or that we are in a concentration range where the state of aggregation is not changing".

NMR Results

A 0.7 M solution of **56** (enriched with ^{6}Li) in THF-d_8 at +25 °C shows one signal each in the ^{1}H, ^{13}C, and ^{6}Li NMR spectrum ($\delta_{^1H}$ = 5.58 ppm, $\delta_{^{13}C}$ = 103.56 ppm, $\delta_{^6Li}$ = −8.60 ppm). When a 1.54 M solution is cooled, the ^{6}Li signal broadens at −90 °C and splits into two resonances at −107 °C (Figure 12).

One chemical shift at −13.10 ppm is very similar to that found for the dimer sandwich **6** of Li-isodiCp (see Figure 8). We therefore conclude that CpLi **56** behaves similarly to Li-isodiCp **1** and exists as a monomer–dimer equilibrium in THF-d_8 at low temperatures. The second ^{6}Li peak at −6.30 ppm found for **56** in THF-d_8 at the lowest accessible temperature (−121 °C, a strongly supercooled solution) still appears to be due to an averaged signal. This peak corresponds to the coalesced signal of the analogous −1.10 and −7.64 ppm peaks of the similar Li-isodiCp spectra of Figure 8. Thus, the spectrum at −121 °C (152 K) of Figure 12 would correspond to the spectrum at −80 °C (193 K) of Figure 8.

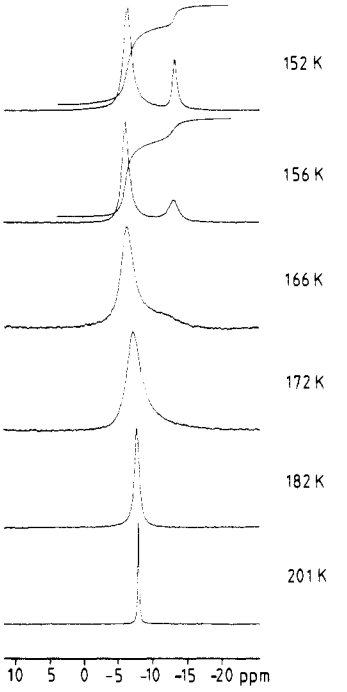

Figure 12. Temperature-dependent ^{6}Li NMR spectra of ^{6}LiCp **38** in THF-d_8, 1.54 M.

Accordingly, kinetic schemes of exchange analogous to Schemes II and III also should hold for CpLi. However, as the coalescence temperatures are considerably lower than those for Li-isodiCp, the exchange rates must be much larger than those found for **1**.

The ^{1}H NMR spectrum of **56** in THF-d_8 agrees well: below −110 °C two signals are found in an approximate 3:2 ratio at δ = 5.59 ppm (monomer) and δ = 5.26 ppm (dimer; 1.54 M solution). Likewise, the ^{13}C NMR spectrum at −121 °C shows a minor peak at 103.65 ppm (dimer) and a major peak at 102.60 ppm (monomer).

At room temperature an averaged monomer–dimer equilibrium might be present. Variation of the concentration would not lead to drastic changes in the ^{1}H and the ^{13}C NMR spectra due to the similarity of the monomer and dimer chemical shifts. Likewise, the single ^{6}Li NMR peak observed at room temperature might arise either from a single aggregate or from a monomer–dimer equilibrium. Thus, from the data obtained we cannot tell whether the monomer–dimer equilibrium of **56** at low temperatures is shifted to either side at room temperature.

MNDO Calculations

All calculational studies[49–56] describe CpLi as having the metal placed symmetrically above the five-membered ring. The fully

(49) Wardell, J. L. In *Comprehensive Organometallic Chemistry*; Wilkinson, G., Stone, F. G. A., Abel, E. W., Eds.; Pergamon: Oxford, 1982; Chapter 2.
(50) Jemmis, E. D.; Schleyer, P. v. R. *J. Am. Chem. Soc.* **1982**, *104*, 4781.
(51) Preuss, H.; Diercksen, G. *Int. J. Quantum Chem.* **1967**, *1*, 349.
(52) Dewar, M. J. S.; Haddon, R. C. *J. Am. Chem. Soc.* **1973**, *95*, 5836.
(53) Anh, N. T.; Elian, M.; Hoffmann, R. *J. Am. Chem. Soc.* **1978**, *100*, 110.
(54) Alexandratos, S.; Streitwieser, A., Jr.; Schaefer, H. F., III *J. Am. Chem. Soc.* **1976**, *98*, 7959.
(55) Lattmann, M.; Cowley, A. H. *Inorg. Chem.* **1984**, *23*, 241.
(56) Waterman, K. C.; Streitwieser, A., Jr. *J. Am. Chem. Soc.* **1984**, *106*, 3138.

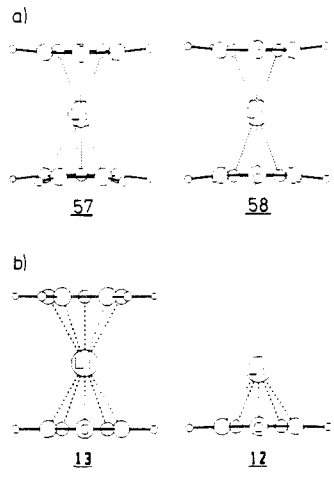

Figure 13. (a) MNDO optimized geometries of "staggered" (**57**) and "eclipsed" (**58**) $[Cp_2Li]^-$ (side view). (b) Ab initio (3-21G) calculated structures of "staggered" $[Cp_2Li]^-$ **13** and CpLi **12** (side view).

optimized MNDO structures of the sandwich dimer anion $[(Cp)_2Li]^-$, **57** and **58** (Figure 13a), with staggered and with eclipsed Cp rings, have identical energies ($\Delta H°_f$ = −45.7 kcal/mol) and adopt D_5 symmetry. Thus, **57** and **58** deviate slightly from perfectly staggered (D_{5d}) and eclipsed (D_{5h}) structures.

A frequency calculation for both conformers revealed only negligible negative eigenvalues (**57**, −2.3 cm^{-1}; **58**, −9.7 cm^{-1}). This indicates essentially free rotation of the Cp rings around the longitudinal axis in the sandwich dimer anion.

A side view at both structures (**57** and **58**, Figure 13a) shows the hydrogen atoms to be bent "outward" (8° deviation from the C_5 plane). Similar findings for CpLi obtained by ab initio calculations were reported earlier by Streitwieser.[56] This was attributed to the enhanced negative charge put toward the cation achieved by outward bending of the hydrogens.

However, ab initio (3-21G) calculations on CpLi (3-21G[50] and 6-31G*[57]) and $[Cp_2Li]^-$ (3-21G) give results different from the MNDO structures. Whereas the outward bending of the hydrogen atoms (2° from the C_5 plane) is present in CpLi (**12**, Figure 13b), no such effect is found in $[Cp_2Li]^-$ (**13**, Figure 13b). Rather, the hydrogen atoms lie almost exactly in the C_5 plane for this species (sum of the bond angles, 360° at carbon).

The discrepancy between the MNDO and the ab initio results is certainly due to the overestimation of the C–Li bond strength by MNDO.[42] Thus, MNDO yields a C–Li distance of 2.323 Å for the sandwich ions **57** and **58** whereas in the ab initio calculation a distance of 2.368 Å is found. In contrast, r_{C-Li} is considerably shorter in monomeric CpLi (3-21G, 2.157 Å; 6-31G*, 2.133 Å[57]).

Conclusions

Both an exo lithium isocyclopentadienide monomer **4** and a related bis exo dimer sandwich **6** coexist in THF solution at low temperatures. This was demonstrated by experimental (NMR, cryoscopy) as well as by calculational (MNDO, IGLO) methods. The differences in exo vs endo stereoselectivity in the reactions of Li–isodiCp **1** with electrophiles are apparently due to changes in the state of aggregation with different temperatures.

New and unexpected results were obtained for CpLi **56** at very low temperatures. Similar to **1**, CpLi was found to consist of a monomer–dimer equilibrium in THF-d_8.

The present study demonstrates the efficiency of a combination of experimental and calculational methods for the structure analysis of organolithium compounds.

Experimental Section

All experiments involving organolithium compounds were carried out in flame-dried glassware under an atmosphere of dry argon.

Synthesis of **1**: In a 30-mL flask was placed 1.03 g (7.78 mmol) of isodicyclopentadiene[1] dissolved in small amounts of diethyl ether. The solvent was removed in vacuo and replaced by 12 mL of dry hexane. With stirring, 3.2 mL (8.0 mmol) of ^{6}Li-enriched butyllithium[21] in hexane (2.49 M) was slowly added, followed by slow addition of 11 mL of diethyl ether. After stirring for 24 h at room temperature, the white precipitate was filtered off (D4 porosity filter stick), washed with two 5-mL portions of hexane, and dried in vacuo.

^{6}LiCp **56** was synthesized by adding 1 equiv of ^{6}Li-enriched *n*-butyllithium in hexane[21] to a solution of 958 mg (14.5 mmol) of freshly cracked dicyclopentadiene in hexane. After addition of 8 mL of diethyl ether, the white precipitate was filtered off, washed with hexane, and dried in vacuo.

NMR spectra were recorded on a JEOL GX400 spectrometer under conditions previously described.[8,29] ^{1}H and ^{13}C NMR spectra are referenced to the internal solvent signals: δ = 3.58 ppm (^{1}H, THF-d_7, α-H) and δ = 67.4 ppm (^{13}C, THF-d_8, α-C); ^{6}Li NMR spectra are referenced to 1 M LiBr in THF/THF-d_8; the reference measurements were carried out separately prior to the actual measurements at the appropriate temperatures.

The one-dimensional difference NOE spectrum (Figure 2) was recorded with a spectral width of 2331 Hz, 16K data points, 90° pulse, 64 scans, and 5-s preirradiation time.

Selected parameters of the 2D NMR spectra are as follows.

COSY (Figure 3): spectral width 2331 Hz (f_1, f_2), 90° pulse length 18 μs, 1024 data points in t_2, 64 increments in t_1 with 64 scans per increment, one times zero filling in both t_1 and t_2, unshifted sine-bell window in t_1 and t_2.

C,H shift correlation (Figure 4): ^{1}H 90° pulse width 15 μs, ^{13}C 90° pulse width 9 μs, spectral width 2331 Hz (f_1) and 13 020 Hz (f_2), 1024 data points in t_2, 128 increments in t_1 with eight scans per increment, one times zero filling in both t_1 and t_2, Gaussian window in t_1 and t_2.

ROESY (Figure 6): spectral width 2331 Hz (f_1, f_2), 90° pulse width 37.5 μs (attenuated). Pulsed spin-lock was achieved by a repeated (30° pulse 125-μs)$_n$ sequence with n = 504 (equal to a mixing time of 70 ms) as was described by Kessler.[58] Exponential line broadening in t_1 and t_2, 1024 data points in t_2, 128 t_1 increments with 32 scans per increment, one times zero filling in both t_1 and t_2. Pure absorption representation (Ruben, States, Haberkorn method for quadrature detection in f_1; cf. ref 6).

^{6}Li,^{1}H HOESY (Figure 7): spectral width 1200 (^{6}Li, f_2) and 2331 Hz (^{1}H, f_1), 512 data points in t_2, 128 t_1 increments with 32 scans per increment, mixing time 1.1 s, exponential line broadening in t_2, Gaussian window in t_1, two times zero filling in t_1; pure absorption representation (Ruben, States, Haberkorn method for quadrature detection in f_1; cf. ref 6).

In no case were symmetrization procedures carried out, COSY and C,H shift correlation spectra are shown in the magnitude mode.

IGLO calculations were performed on a Convex C 120 computer. A Huzinaga[59] basis set of double ζ (DZ) quality was used, which is contracted as follows:[23] C, 7s3p contracted to 4111,21; Li, 7s contracted to 4111; H, 3s contracted to 21. Structure **13** was optimized with the CADPAC[60] program by employing a standard 3-21G basis set.[61,62]

MNDO calculations were carried out on the CONVEX using the VAMP4 (vectorized ampac) program. Unless otherwise noted, all geometry optimizations were done without symmetry restrictions by using the keyword PRECISE, which increases the accuracy of criteria by a factor of 10–100.

Cryoscopic measurements were made using a modification of the apparatus described by Seebach.[25]

Acknowledgment. We thank G. Fraenkel for helpful discussions, T. Clark for the VAMP4 program, W. Kutzelnigg and M. Schindler for the CONVEX version of the IGLO program, D. Seebach for loan

(57) Bühl, M.; Schleyer, P. v. R. Unpublished results.

(58) Kessler, H.; Griesinger, C.; Kerssebaum, R.; Wagner, K.; Ernst, R. R. *J. Am. Chem. Soc.* **1987**, *109*, 607.
(59) Huzinaga, S. *Approximate Atomic Wave Functions*; University of Edmonton: Edmonton, AB, Canada, 1971.
(60) Amos, R. D.; Rice, J. E. *CADPAC*: The Cambridge Analytic Derivatives Package, Issue 4.0; Cambridge, 1987.
(61) Binkley, J. S.; Pople, J. A.; Hehre, W. J. *J. Am. Chem. Soc.* **1980**, *102*, 939.
(62) Gordon, M. S.; Bintley, J. S.; Pople, J. A.; Pietro, W. J.; Hehre, W. J. *J. Am. Chem. Soc.* **1982**, *104*, 2797.
(63) Stults, S. S.; Andersen, R. A.; Zalkin, A. *J. Am. Chem. Soc.* **1989**, *111*, 4507.
(64) Bhide, V.; Rinaldi, P.; Farona, M. F. *J. Organomet. Chem.* **1989**, *376*, 91.
(65) Bhide, V. V.; Rinaldi, P. L.; Farona, M. F. *Organometallics* **1990**, *9*, 123.
(66) den Besten, R.; Harder, S.; Brandsma, L. *J. Organomet. Chem.* **1990**, *385*, 153.
(67) Hertkorn, N.; Köhler, F. H. *Z. Naturforsch.* **1990**, *45B*, 848.

of the cryoscopy apparatus, and P. Gregory for some MNDO calculations. Financial support from the Deutsche Forschungsgemeinschaft, the Fonds der Chemischen Industrie, and the Convex Computer Corp. is gratefully acknowledged. M.R.S. would like to thank the U.S. Department of Education for a National Needs Fellowship.

Note Added in Proof. Since submission of this manuscript, a number of papers pertinent to the title compounds have been published. Andersen et al.[63] described the crystal structure of $[Li(TMEDA)_2][Li_2(TMEDA)_2\text{-}\mu\text{-}n^5,n^5\text{-}MeC_5H_4][n^5\text{-}MeC_5H_4)_6U_2(\mu\text{-}Me)]_2$. Therein, the linear Li–MeCp–Li cation can be thought of as an inverse of sandwich **6**. Farona et al.[64] analyzed the iron derivative of isodiCp and its dehydro isomer **46** by means of two-dimensional NMR. All possible exo/exo, exo/endo, and endo/endo isomers of both species were studied. The same group also describes 2D NMR studies of the analogous Ti and Zr derivatives.[65] Brandsma et al. determined the degree of aggregation of CpLi in liquid ammonia by means of cryoscopy.[66] A monomer–dimer equilibrium (60:40) was detected. This agrees favorably with our NMR findings described above. Köhler et al.[67] recorded the ^{13}C NMR spectra of lithium and potassium bicyclo[3.2.1]octa-2,6-dienide. Whereas the potassium compound is a CIP, a CIP–SSIP equilibrium was detected for the lithium compound, very similar to our findings described in this paper.

UV Resonance Raman Saturation Spectroscopy Measures Protein Aromatic Amino Acid Excited State Relaxation Rates

Paul A. Harmon, Junji Teraoka,† and Sanford A. Asher*

Contribution from the Department of Chemistry, University of Pittsburgh, Pittsburgh, Pennsylvania 15260. *Received February 16, 1990*

Abstract: We demonstrate the utility of the new technique of UV resonance Raman saturation spectroscopy (Teraoka et al. *J. Am. Chem. Soc.* **1990**, *112*, 2892) for studying tryptophan and tyrosine excited-state relaxation rates in proteins. This technique monitors the ground-state population during UV pulsed laser excitation. It reports on ground-state recovery rates for aromatic amino acid residues which depend upon energy-transfer processes and photoionization quantum yields. We demonstrate the dependence of the relaxation rates on aromatic amino acid environment in lysozyme, myoglobin, and glucagon and examine energy transfer between aromatic amino acid residues in a tryptophan–tyrosine dimer. In contrast to aromatic amino acid solution studies, we find little photoionization in the proteins studied. This technique is of general utility for studying relaxation rates of chromophores, even those with weak fluorescence such as phenylalanine and tyrosine in proteins containing tryptophan residues. We discuss the utility of this technique for future biological and chemical applications. We also demonstrate the dependence of the aromatic amino acid residue Raman cross sections to the protein residue environment.

Introduction

The establishment of molecular structure and function relationships in biomolecules is hindered by the size and complexity of these systems. A host of techniques has been developed and applied to examine different facets of molecular structure and dynamics for these macromolecules.[1,2] For example, X-ray diffraction, NMR, CD, and numerous other spectroscopies have been applied to studying various aspects of protein structure in order to define enzymatic mechanisms at the molecular level. An incisive glimpse into the enzymatic mechanism generally results only from combining the information derived from each separate approach. Thus, the development of new techniques for studying biomolecular structure is crucial for progress in biochemistry and biophysics; as more information is obtained, more detailed molecular questions can be posed.

A number of powerful optical spectroscopic techniques have focused on the UV spectral region,[3] such as UV absorption spectroscopy, fluorescence spectroscopy, and UV CD spectroscopy. Absorption techniques have concentrated on studying aromatic amino acid residues such as tryptophan (TRP), tyrosine (TYR), and phenylalanine (PHE) in proteins, while fluorescence studies of proteins have been limited primarily to TRP residues.[4-8] The importance of these results derives from the valuable information obtained on the protein structure by probing the aromatic amino acid environments. The power of TRP residue fluorescence lifetime measurements, for example, rests on the exquisite sensitivity of excited-state relaxation rates to the immediate fluorophore environment. UV resonance Raman spectroscopy (UVRR) has recently shown the ability to selectively examine the vibrational spectra of all three aromatic amino acids in proteins.[9-11] The utility of UVRR is based on the wavelength dependence of the resonance effect and the dependence of the Raman vibrational frequencies on the residue environment.[9-13] In addition, we recently demonstrated a new technique, UVRR saturation spectroscopy,[14] that uses UVRR intensities to monitor the aromatic amino acid relaxation rates back to the ground state. This previous

* Author to whom correspondence should be addressed.
† Present address: Osaka City University, Osaka, Japan.

(1) See, for example: Biophysics; Hoppe, W., Lohmann, W., Markl, H., Ziegler, H. Eds.; Springer-Verlag: Heidelberg, 1983.
(2) Cantor, C. R.; Schimmel, P. R. Biophysical Chemistry; Bartlett, A. C., Vapnek, P. C., McCombs, L. W., Eds.; W. H. Freeman and Co.: 1980; Vol. II.
(3) Demchenko, A. P. Ultraviolet Spectroscopy of Proteins; Springer-Verlag: Berlin, 1986.
(4) Beechem, J. M.; Brand, L. *Ann. Rev. Biochem.* **1985**, *54*, 43.
(5) Longworth, J. W. In *Time Resolved Fluorescence Spectroscopy in Biochemistry and Biology*; Cundall, R. B., Dale, R. E. Eds.; Plenum: London, 1983; p 651.
(6) Lakowicz, J. R. In *Principles of Fluorescence Spectroscopy*; Plenum: New York, 1983.
(7) Petrich, J. W.; Longworth, J. W.; Fleming, G. R. *Biochemistry* **1987**, *26*, 2711.
(8) Hutnik, C. M.; Szabo, A. G. *Biochemistry* **1989**, *28*, 3923, 3935.
(9) Asher, S. A. *Ann. Rev. Phys. Chem.* **1988**, *39*, 537.
(10) Harada, I.; Takeuchi, H. In *Spectroscopy of Biological Systems*; Clark, R. J. H., Hestor, R. E., Eds.; John Wiley and Sons: 1986; Chapter 3.
(11) Spiro, T. G.; Grygon, C. A. *J. Mol. Struct.* **1988**, *173*, 79.
(12) Su, C.; Park, Y. D.; Lui, G.-Y.; Spiro, T. G. *J. Am. Chem. Soc.* **1989**, *111*, 3457.
(13) Kaminiaka, S.; Ogura, T.; Kitagawa, T. *J. Am. Chem. Soc.* **1990**, *112*, 23.

0002-7863/90/1512-8789$02.50/0